이학석사 학위논문

Synthesis and Analysis of Graphene Quantum Dots and Their Therapeutic Applications to Ulcerative Colitis

그래핀 양자점 합성 및 분석과 염증성 장질환에서의 적용

2021년 2월

서울대학교 대학원

화학부 물리화학 전공

김 주 희

Synthesis and Analysis of Graphene Quantum Dots and Their Therapeutic Applications to Ulcerative Colitis

Advisor: Byung Hee Hong

Submitting a M.S. Dissertation of Chemistry

February 2021

Graduate School of Natural Sciences

Seoul National University

Chemistry Major

Juhee Kim

Confirming the M.S. Dissertation written by Juhee Kim

November 2020

Chair	Jwa-Min Nam	(Seal)
Vice Chair	Byung Hee Hong	(Seal)
Examiner	Yan Lee	(Seal)

Abstract

Synthesis and Analysis of Graphene Quantum Dots and Their Therapeutic Applications to Ulcerative Colitis

Juhee Kim

Department of Chemistry

The Graduate School

Seoul National University

Graphene-based nanomaterials (GBNs) have been applied in the photocatalyst, displays, energy storage devices due to tunable properties and stability. Among them, graphene oxides (GOs) and graphene quantum dots (GQDs) exert high biocompatibility and low toxicity, depending on their characteristics. Besides, due to the superb antioxidant effect, GBNs can scavenge radical oxygen species and have been applied to numerous inflammatory diseases. As the toxicity depends on various factors such as size, surface charge, and concentration, it is essential to control and functionalize for the appropriate usage. Some GBNs emit high intensity of photoluminescence, facilitating their usage in bioimaging. Due to the large surface area, they have also been used as cargo for drug delivery. Recently, GQDs have been proved to interact with the pathogenic protein α-synuclein physically. GQDs degraded preformed fibrils and even inhibited the fibrils' formation when co-incubated with monomers, suggesting a new therapy method for Parkinson's disease. Based on the numerous applications of GQDs on diseases, this dissertation describes the synthesis and characterization of GQDs of two sizes and their applications to ulcerative colitis.

Chapter 1 starts by describing the synthesis and characterization of large and small GQDs. Focusing on the biomedical application of GQDs, the antioxidant ability and antibacterial effect of GOs and GQDs are explained. Next, the application of GQDs in various disease models is introduced, including a brief description of ulcerative colitis. As GQDs' biocompatibility and toxicity vary, we stressed that the toxicity differs by physicochemical properties and administration route. Lastly, some surface modification methods, such as conjugating small molecules to GQDs, are explained.

Chapter 2 describes the application of GQDs of relatively large size as the alternative therapeutic agent for ulcerative colitis, one of the inflammatory bowel diseases (IBDs). This research was done by collaborating with the college of veterinary medicine, Seoul National University. GQDs were intraperitoneally (i.p.) injected into the DSS (Dextran Sodium Sulfate)-induced colitis model. GQDs alleviated excess inflammation and, through interaction with immune cells, able to restore immune homeostasis. When GQDs were treated to the healthy mice, no significant toxicity was found, with verification of safe clearance through urine.

Chapter 3 is about applying small-sized GQDs to the same colitis model through oral delivery. Again, GQDs did not exert significant toxicity despite their different size and administration route. Considering the exposure of GQDs to acidic conditions such as gastric acid, we dispersed GQDs in HCl solution and analyzed the change in characteristics. Overall, GQDs of both sizes and administration routes showed the potential to be used as a treatment for IBDs.

Key words: Graphene, graphene-based nanomaterials, graphene oxides, graphene quantum dots, inflammatory bowel diseases, ulcerative colitis

Student number: 2018-26779

Table Contents

Abstract of Dissertation i

List of Figures and Tables v

Chapter 1. Properties and applications of graphene quantum dots

1.1. Synthesis and Characterization of GQDs 1

1.1.1. Synthesis and characterization of large GQDs 1

1.1.2. Synthesis and characterization of small GQDs 3

1.2. Properties of GQDs 4

1.2.1. Antioxidant ability of graphene-based nanomaterials 4

1.2.2. Antibacterial effect of graphene-based nanomaterials 5

1.3. Application of GQDs 6

1.3.1 Biomedical application of GQDs 7

1.3.2 Application of GQDs to ulcerative colitis 8

1.4. Biocompatibility and toxicity of GQDs 9

1.4.1 Toxicity of GQDs depends on various properties 9

1.4.2 Toxicity depending on delivery route 10

1.5. Surface modification and further analysis of GQDs 10

1.5.1. Conjugation of biotin to GQDs 10

1.5.2. Conjugation of rhodamine to GQDs 12

1.6. References 14

Chapter 2. Graphene quantum dots as anti-inflammatory therapy for colitis

2.1. Introduction.....17

2.2. Results.....22

2.3. Discussion.....24

2.4. Methods.....26

2.5. References.....29

Chapter 3. Oral administration of microbiome-friendly graphene quantum dots as therapy for colitis

3.1. Introduction.....31

3.2. Results.....34

3.3. Discussion.....51

3.4. Methods.....54

3.5. References.....62

Appendix.....67

Abstract in Korean.....69

List of Figures and Tables

Chapter 1

Fig. 1-1. Characterization of GOs.

Fig. 1-2. Characterization of large GQDs.

Fig. 1-3. The HR-TEM image of GQDs from the batch-up synthesis method.

Fig. 1-4. The synthesis and characterization of GQDs.

Fig. 1-5. Mechanism of the antioxidant ability of GQDs. Reprinted from reference 10, © 2017 Elsevier Ltd.

Fig. 1-6. The antibacterial effect of GOs. Reprinted from reference 12, © 2019 Elsevier B.V.

Fig. 1-7. GQDs exhibit anti-fibrotic ability towards α-synuclein. Reprinted from reference 19, © 2018 Springer Nature

Fig. 1-8. The method of conjugating biotin to GQDs.

Fig. 1-9. The FT-IR spectra of pristine and biotin-conjugated GQDs.

Fig. 1-10. The biotin-streptavidin assay analysis of large GQDs cleared through urine. Reprinted from reference 31, © 2020 American Association for the Advancement of Science

Fig. 1-11. The UV-Vis absorbance spectrum of pristine GQDs.

Fig. 1-12. The synthesis of GQDs-NH_2.

Fig. 1-13. The photoluminescence spectrum of pristine GQDs and GQDs-Rhodamine excited at 490 nm and 550 nm, respectively.

Fig. 1-14. The confocal image of GQDs and GQDs-Rhodamine treated MEF cells.

Chapter 2

Fig. 2-1. Intraperitoneal injection of GQDs effectively alleviates DSS-induced chronic colitis in mice.

Fig. 2-2. GQDs are excreted from mice without generating toxicity.

Fig. 2-3. Synthesis and characterization of GQDs.

Fig. 2-4. Schematic diagram of the GQDs' effect on colitis.

Table 2-1. Elemental Analysis of GQDs

Chapter 3

Fig. 3-1. Synthesis and physicochemical characteristics of GQDs after acid exposure.

Fig. 3-2. Characterization of GQDs.

Fig. 3-3. Intraperitoneal injection of GQDs suppress DSS-induced colitis in mice.

Fig. 3-4. Oral administration of GQDs alleviates DSS-induced colitis.

Fig. 3-5. Effects of GQDs on colonic inflammation and inflammatory cytokines in serum.

Fig. 3-6. GQDs suppress immune cell activity.

Fig. 3-7. GQDs have an effect on the $CD4^+$ T cells.

Fig. 3-8. GQDs suppress M1 macrophage's activity.

Fig. 3-9. Oral administration of GQDs does not exert toxic effects.

Fig. 3-10. Characterization of GOs.

Table 3-1. Quantitative RT-PCR primers

Chapter 1

Properties and applications of graphene quantum dots

1.1. Synthesis and Characterization of GQDs

This part will examine how to synthesize and analyze large and small graphene quantum dots (GQDs) and figure out their physical and chemical characteristics. Among various synthesis methods, large GQDs were made by breaking down graphene oxides (GOs), and small GQDs were synthesized by the thermo-oxidation cutting of carbon fiber. The characterization of GQDs was done by TEM, AFM, Raman spectroscopy, FT-IR, and XPS.

1.1.1. Synthesis and characterization of large GQDs

Large GQDs were synthesized by first synthesizing GOs, according to the improved Hummer's method (*1*). Briefly explaining, graphite powder was mixed with H_2SO_4, H_3PO_4, and $KMnO_4$ and reacted at 50 ^oC for 24 hours. After complete cooling, H_2O_2 was slowly poured in and gently mixed until the solution turns in to light yellow. After diluting with deionized (DI) water, we removed acid by multiple washing through a centrifugation. Then the GOs solution was freeze-dried to obtain GOs powder. The particle size was measured by FE-SEM, in which GOs had a broad size distribution of 5.09±2.47 μm (Fig. 1-1A). The functional groups were analyzed by FT-IR, showing GOs consist of hydroxyl, carboxyl, and epoxide groups with a graphitic domain (Fig. 1-1B).

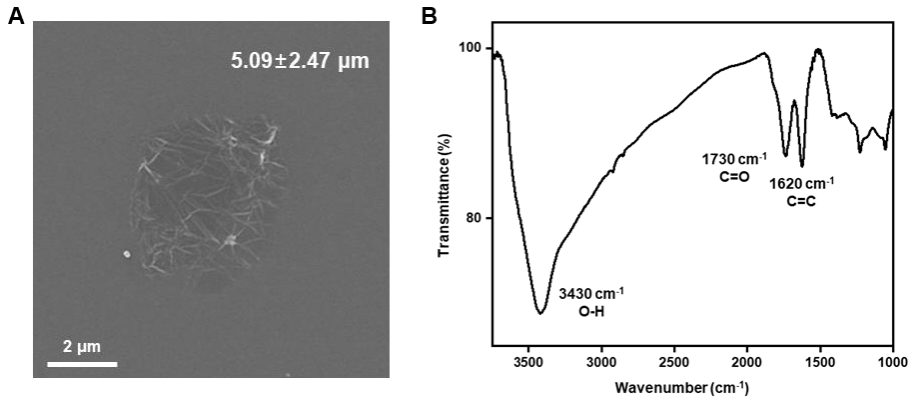

Fig. 1-1. Characterization of GOs. (**A**) The FE-SEM image and (**B**) the FT-IR spectrum of GOs.

Then, large GQDs were made by breaking down GOs with tip-sonication. By controlling GOs solution concentration and the sonication time, the large GQDs of size 20~30 nm were obtained (Fig. 1-2A). Again, FT-IR analysis was carried on to verify the oxidized structure of large GQDs (Fig. 1-2B).

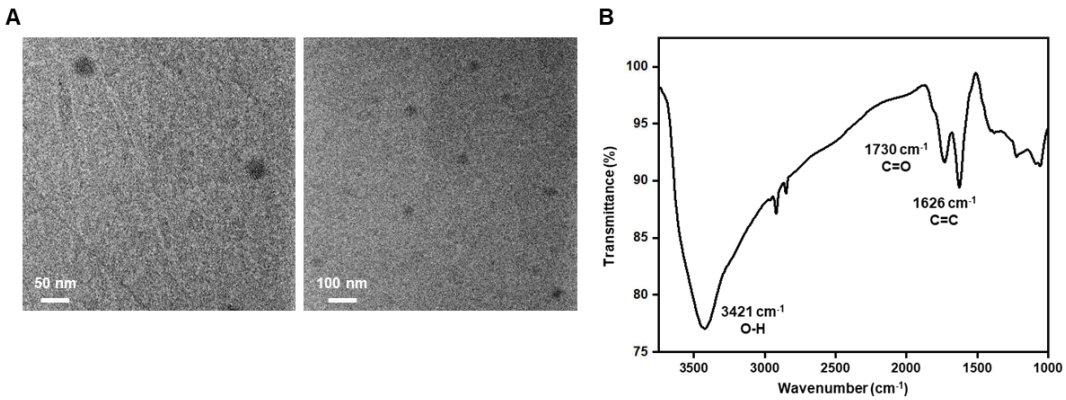

Fig. 1-2. Characterization of large GQDs. (**A**) The HR-TEM image and (**B**) the FT-IR spectrum of large GQDs.

1.1.2. Synthesis and characterization of small GQDs

Small GQDs were synthesized by thermo-oxidation cutting of carbon fiber (*2*). Carbon fiber was mixed with H_2SO_4 and HNO_3 at a volume ratio of 3:1, and the mixture solution was vigorously stirred for 24 hours at 80 ^oC. After complete cooling, the mixture was diluted by DI water of 10 times its volume, and by using 1 kDa dialysis tube, the remaining acids were removed. After filtering, removal of the excess solvent, and freeze-drying, the powder form of GQDs were obtained.

In order to synthesize more volume of GQDs at once, we increased the total volume of the mixture, and the increase in temperature was necessary. When the solution batch was doubled, and by increasing the temperature to 90 ^oC, GQDs of ~ 5 nm were obtained (Fig. 1-3A). However, when increasing the volume up to 3 times and raising the temperature to 110 ^oC, the GQDs of 2~3 nm with similar characteristics of GQDs made by a single batch was gathered (Fig. 1-3B).

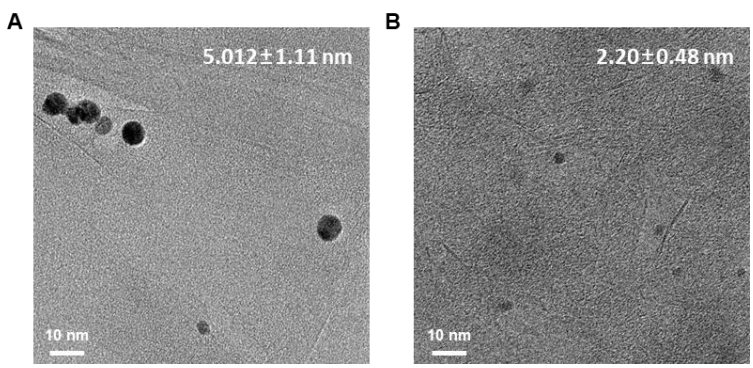

Fig. 1-3. The HR-TEM image of GQDs from the batch-up synthesis method. (**A**) GQDs synthesized by the double volume, at 90 ^oC and (**B**) the triple batch synthesized at 110 ^oC.

Next, detailed analysis of GQDs were carried on. By the thermo-oxidation cutting of carbon fiber (Fig. 1-4A), GQDs of 2~3 nm were obtained (Fig. 1-4B). The thickness was measured by AFM, which is around 1.4 nm, referring to 2~5 layers of the graphene layer (Fig. 1-4C). From the Raman spectroscopy, the G band, referring to the graphitic domain, and the D band, implying defect sites were observed (Fig. 1-4D). Functional groups were analyzed by FT-IR, where the C=C (1620 cm^{-1}), O-H (3440 cm^{-1}), C=O (1720 cm^{-1}), and C-O (1250 cm^{-1}) are the major characteristic

peaks of GQDs (Fig. 1-4E). Quantification of the functional groups was also done by XPS, verifying the highly oxidized structure (Fig. 1-4F).

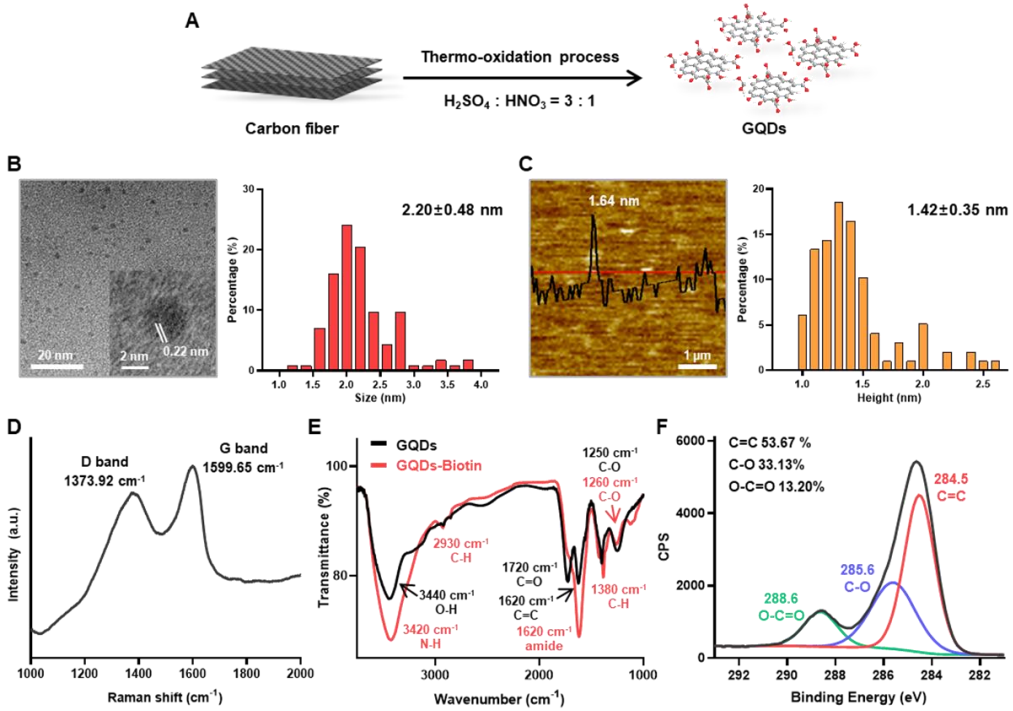

Fig. 1-4. The synthesis and characterization of GQDs. (**A**) The schematic drawing of GQDs synthesis procedure. (**B**) The representative HR-TEM image of GQDs with size distribution. (**C**) The representative AFM image and the height distribution. (**D**) The Raman, (**E**) FT-IR, and (**F**) XPS spectrum of GQDs.

1.2. Properties of GQDs

The optical and electronic properties of GQDs depend on their sizes and chemical composition (*3, 4*). By tuning the photoluminescence, GQDs have been applied in displays (*5*), optoelectronics (*6*), photocatalyst (*7*), and even as a protecting layer in lithium-sulfur batteries (*8*). Despite this, GQDs also exert antioxidant and antibacterial ability, making it useful to be applied in the biomedical field.

1.2.1. Antioxidant ability of graphene-based nanomaterials

Among graphene derivatives, GOs and GQDs are renowned for their antioxidant ability. They can stabilize surrounding hydroxyl radicals by donating hydrogen

atoms from functional groups, or forming a new adduct on its basal plane (Fig. 1-5). Therefore, graphene-based nanomaterials (GBNs) work as excellent reactive oxygen species (ROS) scavengers and reduce oxidative stress. For example, GOs could prevent the oxidation of a dye by scavenging hydroxyl radicals generated from hydrogen peroxide and Fenton's reagent. The electron paramagnetic resonance spectroscopy signal was also decreased by GOs, dose-dependently, exerting protective effect on DMPO oxidation (*9*).

Tuning the antioxidant ability of GQDs is also available through structure modification (*10*). By increasing the sp^2 carbon content, hydrogen atom donating groups, and adding electronegative heteroatoms such as nitrogen, the radical scavenging ability of GQDs was enhanced. Exerting superb antioxidant ability, GQDs have been applied as the therapeutic agents to inflammatory diseases, as excess accumulation of ROS accompanies (*11*).

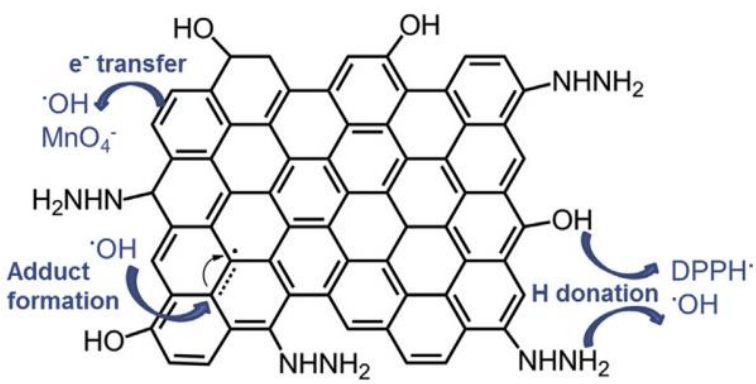

Fig. 1-5. Mechanism of the antioxidant ability of GQDs. Reprinted from reference 10, © 2017 Elsevier Ltd.

1.2.2. Antibacterial effect of graphene-based nanomaterials

GOs are well known for their antibacterial effect. GOs can either physically attack bacteria by the sharp edges; or cover up bacteria, inhibiting growth (Fig. 1-6). Lastly, GOs exert oxidative stress and kill bacteria (*12*). When GBNs are orally delivered, they can affect the microbiome in the intestine. Therefore, verification of

the toxicity towards bacteria is essential before the administration. From the zebrafish model (*13*), GOs, reduced GOs, and monolayer graphene powder caused dysbiosis. The authors stressed that the increase of *Lactobacillus* could be due to the strain's nature to relieve gut inflammation, pointing out the toxic effect of graphene derivatives on the intestinal microbiota. When GOs were treated to high-fat diet-induced hyperlipidemic mice (*14*), they increased short-chain fatty acid (SCFA)-producing bacteria, in which SCFA ameliorates hyperlipidemia by lowering triglycerides level. On the other hand, GQDs derived from GOs do not exhibit an antibacterial effect on their own (*15*). Instead, GQDs were applied to degrade the extracellular matrix of biofilm (*16*) or conjugated with Ag NPs and exposed to blue light to exert ROS and release heat for antimicrobial therapy (*17*).

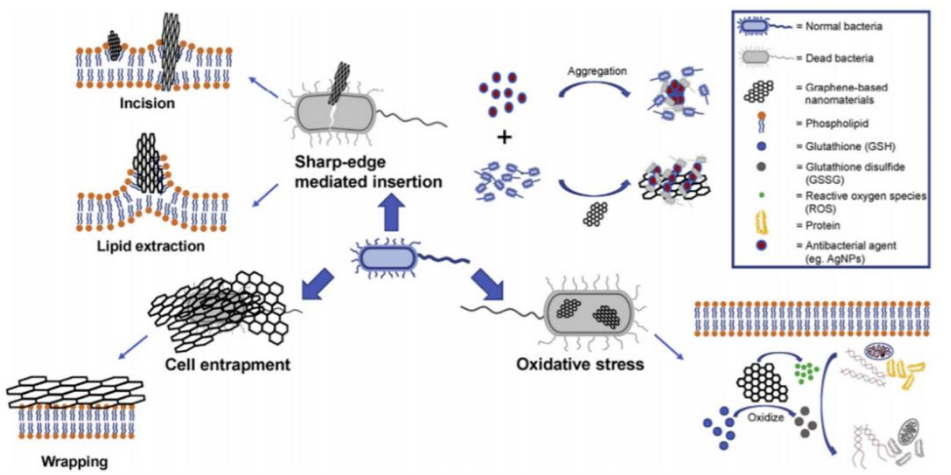

Fig. 1-6. The antibacterial effect of GOs. Reprinted from reference 12, © 2019 Elsevier B.V.

1.3. Application of GQDs

As some GQDs are highly biocompatible without significant toxicity, the biomedical applications of GQDs have gathered attention. GQDs' high surface area and fluorescence facilitate drug delivery and simultaneous tracking (*18*). However, considering the antioxidant ability of GQDs and their interaction with immune cells, using GQDs itself as the therapeutic agent has been extensively researched.

1.3.1. Biomedical application of GQDs

GQDs were applied as the anti-fibrotic therapeutic agent for Parkinson's disease (*19*). The fibrillation of α-synuclein is the main pathogenesis of the disease. When GQDs were co-incubated with the α-synuclein monomers, they prevented the fibrillation (Fig. 1-7A and B). When treated to the preformed fibrils, GQDs successfully disaggregated them (Fig. 1-7C). As GQDs have a negative surface charge, they interact with the N-terminus of the α-synuclein fibrils. Besides, in order to treat Parkinson's disease, the drug must be delivered to the brain, overcoming the blood-brain barrier (BBB). Due to the very small size and amphiphilic characteristics of GQDs, they were able to penetrate BBB and successfully function as the therapeutic agent. As a result, the neuronal and synaptic loss was prevented, improving the motor nerve.

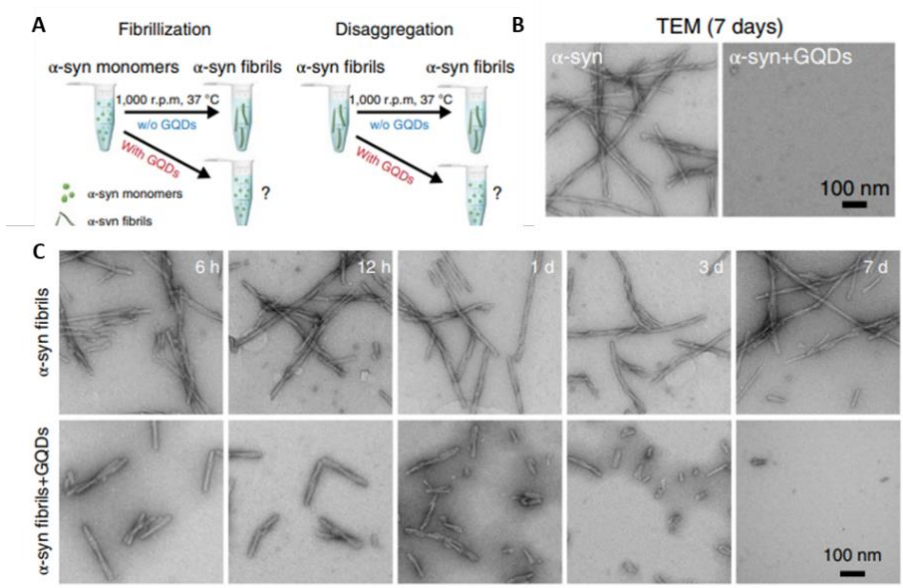

Fig. 1-7. GQDs exhibit anti-fibrotic ability towards α-synuclein. (**A**) GQDs can inhibit fibrillization of α-synuclein monomers and disaggregated preformed fibrils. Representative TEM images of (**B**) the fibrillization of α-synuclein with and without GQDs, and (**C**) GQDs treatment to α-synuclein fibrils at designated time point. Reprinted from reference 19,

Recently, GQDs were applied to treat Niemann-Pick Disease Type C (*20*), one of the lysosomal storage disorders. Due to the inability to degrade cholesterols, they are accumulated in the lysosome, leading to the neuronal dysfunction and

degeneration. As GQDs are amphiphilic material with the hydrophobic basal plane and hydrophilic function groups at the edges, and small enough to enter cells, GQDs were able to internalize to the lysosome and dissolve the aggregated cholesterol. GQDs also promoted autophagy, facilitating the removal of cholesterol.

1.3.2. Application of GQDs to ulcerative colitis

There are 6.8 million inflammatory bowel disease (IBD) patients globally, and the number has been steadily increasing since the 1990s. At first, there was a high incidence of patients in North America and western European countries; therefore, it had been hypothesized that eating habits could cause IBDs (*21*). However, later on, the irrelevance of eating habits was validated, and the disease spread out globally (*22*). There are two types of IBDs; one is Crohn's disease, characterized by patchy inflammation along the intestine, and ulcerative colitis, of which the inflammation is focused at the colon, accompanied by the formation of ulcers. The pathogenesis of colitis is the disruption of epithelium inside the colon, and through the disrupted layer, the pathogenic bacteria flows out, causing inflammation (*23*). The causes of IBDs are weakening in the immune system, genetic or environmental factors; however, an exact cause has not been revealed. The symptoms are inflammation along the large intestine and colon, the formation of ulcers, diarrhea, bleeding, and weight loss. When the symptoms are not too extreme, anti-inflammatory drugs or immune system suppressors are being treated.

IBDs are still not curable, and there are some problems in the current treatment. First, dysbiosis has not been proven to be the direct cause or effect of IBDs, although the phenomenon is observed in the patients (*24*). Therefore, when antibiotics, probiotics, or fecal transplantation were applied, the improvement was not significant or only affected a certain stream of bacteria (*25*). Anti-inflammatory drugs and immune suppressors are commonly prescribed; however, side effects such as weight gain, headache, and bone marrow damage can occur.

As GQDs are highly biocompatible and have the antioxidant ability, they have been applied as alternative therapeutic agents in other inflammatory diseases (*11*). Therefore, GQDs were applied as therapy for colitis, as it accompanies excess inflammation. A detailed explanation of the result is described in Parts 2 and 3.

1.4. Biocompatibility and toxicity of GQDs

The size, surface properties, and concentration of GQDs influence their toxicity and biocompatibility. Therefore, to utilize GQDs as therapeutic agents, it is essential to synthesize highly biocompatible material and find a proper delivery method and optimized concentration.

1.4.1 Toxicity of GQDs depends on various properties

First, the size of GBNs affects toxicity (*26*). Generally, larger GOs exert more toxicity than small-sized GQDs, whereas GQDs of less than 10 nm have high cell viability. Due to their small size, GQDs are quickly and safely cleared out through urine; or degraded by natural enzymes such as horseradish peroxidase and myeloperoxidase (*27, 28*). The concentration of GBNs should also be considered, as a higher dosage increases toxicity.

The surface charge and chemical composition also affect toxicity. When nanoparticles are injected *in vivo*, negatively charged particles are less prone to provoke immune stimulation and inflammation than positively charged ones (*29*). The surface of GBNs is negatively charged due to the oxygen-containing functional groups, making them suitable to be applied in inflammatory diseases. For example, the less oxidized GOs triggered more cytotoxicity due to the increased ROS generation (*30*).

1.4.2 Toxicity depending on delivery route

There are various delivery routes to introduce GQDs *in vivo*. First, when GQDs of size 2~3 nm are intraperitoneally injected, they did not exert long-term toxicity until 6 months and were excreted safely through urine, with a half-life of 2 weeks (*19*). When relatively large GQDs (~20 nm) were injected by the same route, their clearance through urine was also verified (*31*). In the case of GOs, larger GOs caused more inflammation than smaller ones, showing the significance of the size (*32*). When GQDs are intravenously injected, they are also quickly cleared by the kidney (*33*) and did not provoke an increase in inflammatory cytokine level or caused oxidative damage in DNA. Some toxicity was observed when GQDs were orally administered, depending on the material (*34*). When hydroxylated GQDs were administered orally, at high concentration, they suppressed the proliferation of crypt cells and caused oxidative damage in DNA.

Overall, the size and chemical composition of GQDs must be tuned to control biocompatibility and toxicity. GQDs' long-term toxicity should be further examined, and the mechanism of the GQDs' toxicity depending on each physicochemical characteristic should also be analyzed. By doing so, GQDs would be able to function as the therapeutic agent for various incurable diseases.

1.5. Surface modification and further analysis of GQDs

1.5.1. Conjugation of biotin to GQDs

Biotin was conjugated to GQDs to quantify the amount of GQDs excreted or remaining in the kidney through biotin-streptavidin assay (Fig. 1-8). The carboxyl group of GQDs was activated by EDC reagent, and the reaction was carried on in MES buffer to prevent hydrolysis of the agent. After that, NH_2-PEG_3-biotin was added, and dialysis was carried on to remove unreacted molecules.

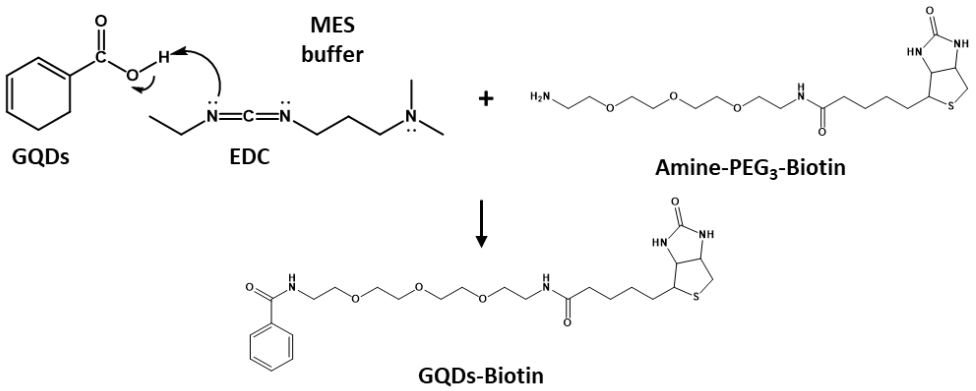

Fig. 1-8. The method of conjugating biotin to GQDs.

The above procedure was applied to both large and small GQDs, of which the success in the reaction was verified by FT-IR spectra (Fig. 1-9). Based on the biotin-streptavidin assay, we were able to figure out the amount of GQDs excreted through urine (Fig. 1-10).

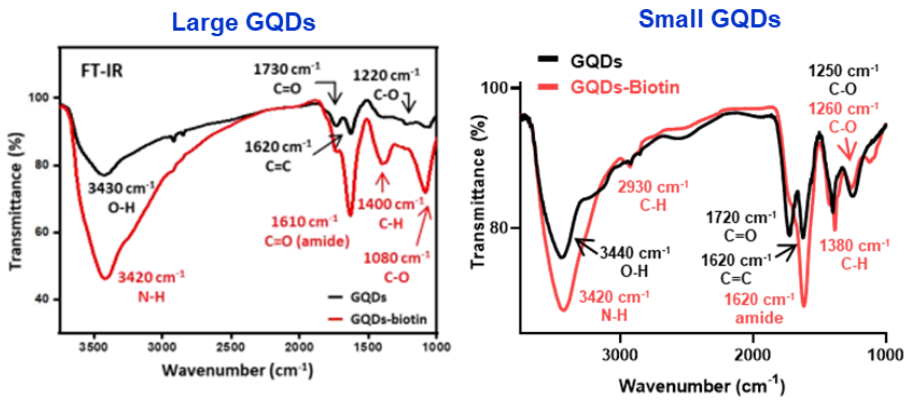

Fig. 1-9. The FT-IR spectra of pristine and biotin-conjugated GQDs.

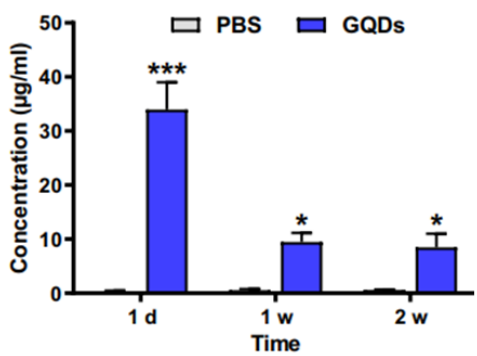

[By Dr. D. Kim / Biographene Inc.]

Fig. 1-10. The biotin-streptavidin assay analysis of large GQDs cleared through urine. Reprinted from reference 31, © 2020 American Association for the Advancement of Science

1.5.2. Conjugation of rhodamine to GQDs

To verify the fate of GQDs after injected *in vivo* and to find out where GQDs are precisely located or where they are more prone to be deposited in organs and tissues, developing a method for tracking GQDs is essential. Although GQDs are known to have inherent fluorescence, the carbon fiber-derived GQDs only emit weak photoluminescence. GQDs highly absorb a wide range of UV-Vis light (Fig. 1-11), and when GQDs are directly attached to the dyes, they quench fluorescence. Therefore, GQDs and rhodamine were conjugated with a PEG linker to prevent quenching of the dye.

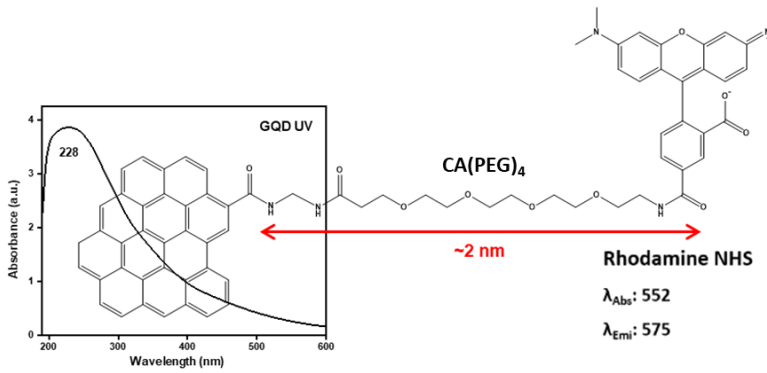

Fig. 1-11. The UV-Vis absorbance spectrum of pristine GQDs.

In order to link GQDs with rhodamine by PEG, first, modification of the carboxyl groups of GQDs was required. After activating the carboxyl group by EDC reagent, NH_2-$(CH_2)_2$-NHBoc was added, and after 24 hours, TFA was added to remove the protecting group (Fig. 1-12). FT-IR was used to verify the success of the reaction.

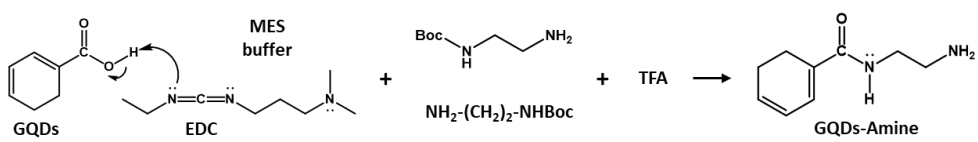

Fig. 1-12. The synthesis of GQDs-NH_2.

As a result, about 10 times of improvement in the intensity of photoluminescence was obtained (Fig. 1-13). When GQDs-Rh were treated to the mouse embryonic fibroblast (MEF) cells, compared to GQDs, we were able to observe GQDs internalized to the cytoplasm (Fig. 1-14).

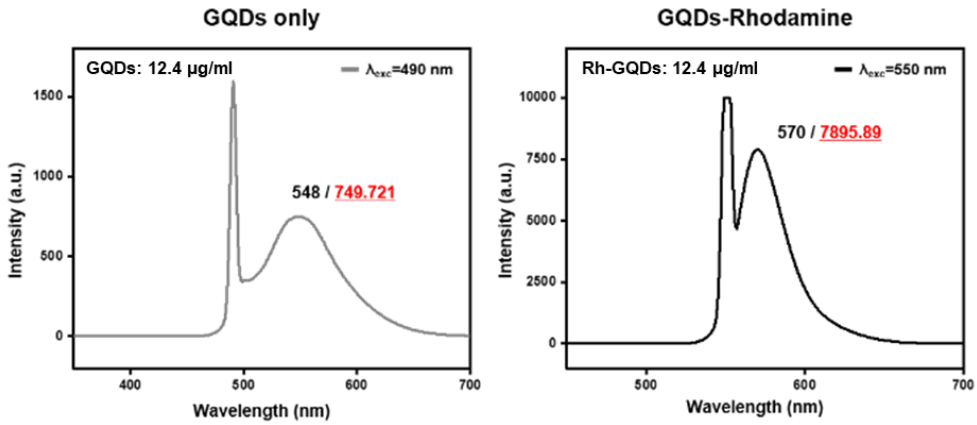

Fig. 1-13. The photoluminescence spectrum of pristine GQDs and GQDs-Rhodamine excited at 490 nm and 550 nm, respectively.

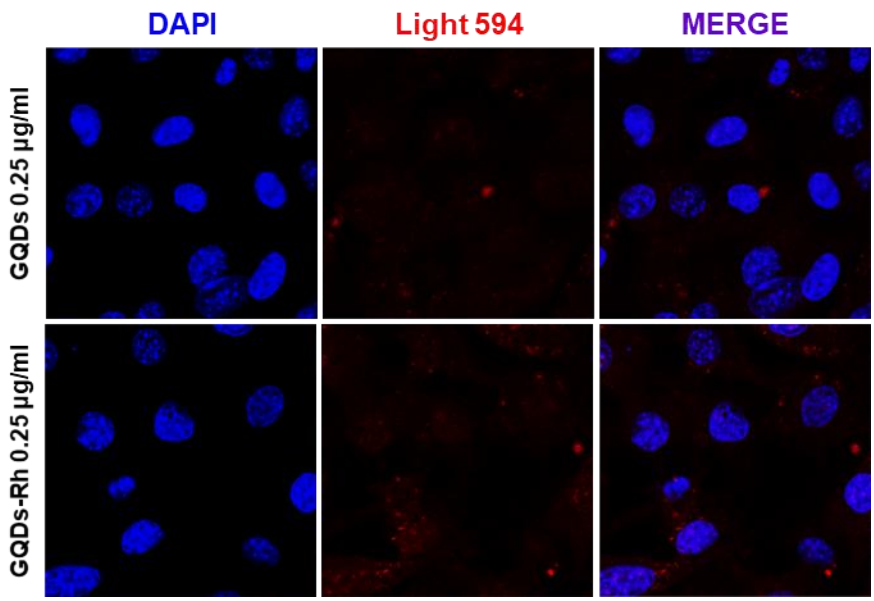

[By. Dr. J. Ahn / Biographene Inc.]

Fig. 1-14. The confocal image of GQDs and GQDs-Rhodamine treated MEF cells.

1.6. References

1. D. C. Marcano, D. V. Kosynkin, J. M. Berlin, A. Sinitskii, Z. Sun, A. Slesarev, L. B. Alemany, W. Lu, J. M. Tour, Improved Synthesis of Graphene Oxide. *ACS Nano* **4**, 4806-4814 (2010).
2. J. Peng, W. Gao, B. K. Gupta, Z. Liu, R. Romero-Aburto, L. Ge, L. Song, L. B. Alemany, X. Zhan, G. Gao, S. A. Vithayathil, B. A. Kaipparettu, A. A. Marti, T. Hayashi, J.-J. Zhu, P. M. Ajayan, Graphene Quantum Dots Derived from Carbon Fibers. *Nano Letters* **12**, 844-849 (2012).
3. S. Kim, S. W. Hwang, M.-K. Kim, D. Y. Shin, D. H. Shin, C. O. Kim, S. B. Yang, J. H. Park, E. Hwang, S.-H. Choi, G. Ko, S. Sim, C. Sone, H. J. Choi, S. Bae, B. H. Hong, Anomalous Behaviors of Visible Luminescence from Graphene Quantum Dots: Interplay between Size and Shape. *ACS Nano* **6**, 8203-8208 (2012).
4. J. Feng, H. Dong, L. Yu, L. Dong, The optical and electronic properties of graphene quantum dots with oxygen-containing groups: a density functional theory study. *Journal of Materials Chemistry C* **5**, 5984-5993 (2017).
5. M. He, X. Guo, J. Huang, H. Shen, Q. Zeng, L. Wang, Mass production of tunable multicolor graphene quantum dots from an energy resource of coke by a one-step electrochemical exfoliation. *Carbon* **140**, 508-520 (2018).
6. J. K. Kim, S. J. Kim, M. J. Park, S. Bae, S.-P. Cho, Q. G. Du, D. H. Wang, J. H. Park, B. H. Hong, Surface-Engineered Graphene Quantum Dots Incorporated into Polymer Layers for High Performance Organic Photovoltaics. *Scientific Reports* **5**, 14276 (2015).
7. Z. Zeng, S. Chen, T. T. Y. Tan, F.-X. Xiao, Graphene quantum dots (GQDs) and its derivatives for multifarious photocatalysis and photoelectrocatalysis. *Catalysis Today* **315**, 171-183 (2018).
8. J. Park, J. Moon, C. Kim, J. H. Kang, E. Lim, J. Park, K. J. Lee, S.-H. Yu, J.-H. Seo, J. Lee, J. Heo, N. Tanaka, S.-P. Cho, J. Pyun, J. Cabana, B. H. Hong, Y.-E. Sung, Graphene quantum dots: structural integrity and oxygen functional groups for high sulfur/sulfide utilization in lithium sulfur batteries. *NPG Asia Materials* **8**, e272-e272 (2016).
9. Y. Qiu, Z. Wang, A. C. E. Owens, I. Kulaots, Y. Chen, A. B. Kane, R. H. Hurt, Antioxidant chemistry of graphene-based materials and its role in oxidation protection technology. *Nanoscale* **6**, 11744-11755 (2014).
10. V. Ruiz, L. Yate, I. García, G. Cabanero, H.-J. Grande, Tuning the antioxidant activity of graphene quantum dots: Protective nanomaterials against dye decoloration. *Carbon* **116**, 366-374 (2017).
11. V. Volarevic, V. Paunovic, Z. Markovic, B. Simovic Markovic, M. Misirkic-Marjanovic, B. Todorovic-Markovic, S. Bojic, L. Vucicevic, S. Jovanovic, N. Arsenijevic, Large graphene quantum dots alleviate immune-mediated liver damage.

Acs Nano **8**, 12098-12109 (2014).

12. M.-Y. Xia, Y. Xie, C.-H. Yu, G.-Y. Chen, Y.-H. Li, T. Zhang, Q. Peng, Graphene-based nanomaterials: the promising active agents for antibiotics-independent antibacterial applications. *Journal of Controlled Release* **307**, 16-31 (2019).
13. M. Zheng, J. Lu, G. Lin, H. Su, J. Sun, T. Luan, Dysbiosis of gut microbiota by dietary exposure of three graphene-family materials in zebrafish (Danio rerio). *Environmental Pollution* **254**, 112969 (2019).
14. J. Li, S. Yang, J. Yu, R. Cui, R. Liu, R. Lei, Y. Chang, H. Geng, Y. Qin, W. Gu, S. Xia, K. Chen, J. Kong, G. Chen, C. Wu, G. Xing, Lipid- and gut microbiota-modulating effects of graphene oxide nanoparticles in high-fat diet-induced hyperlipidemic mice. *RSC Advances* **8**, 31366-31371 (2018).
15. L. Hui, J. Huang, G. Chen, Y. Zhu, L. Yang, Antibacterial Property of Graphene Quantum Dots (Both Source Material and Bacterial Shape Matter). *ACS Applied Materials & Interfaces* **8**, 20-25 (2016).
16. Y. Wang, U. Kadiyala, Z. Qu, P. Elvati, C. Altheim, N. A. Kotov, A. Violi, J. S. VanEpps, Anti-Biofilm Activity of Graphene Quantum Dots via Self-Assembly with Bacterial Amyloid Proteins. *ACS Nano* **13**, 4278-4289 (2019).
17. Y. Yu, L. Mei, Y. Shi, X. Zhang, K. Cheng, F. Cao, L. Zhang, J. Xu, X. Li, Z. Xu, Ag-Conjugated graphene quantum dots with blue light-enhanced singlet oxygen generation for ternary-mode highly-efficient antimicrobial therapy. *Journal of Materials Chemistry B* **8**, 1371-1382 (2020).
18. Q. Duan, Y. Ma, M. Che, B. Zhang, Y. Zhang, Y. Li, W. Zhang, S. Sang, Fluorescent carbon dots as carriers for intracellular doxorubicin delivery and track. *Journal of Drug Delivery Science and Technology* **49**, 527-533 (2019).
19. D. Kim, J. M. Yoo, H. Hwang, J. Lee, S. H. Lee, S. P. Yun, M. J. Park, M. Lee, S. Choi, S. H. Kwon, S. Lee, S.-H. Kwon, S. Kim, Y. J. Park, M. Kinoshita, Y.-H. Lee, S. Shin, S. R. Paik, S. J. Lee, S. Lee, B. H. Hong, H. S. Ko, Graphene quantum dots prevent α-synucleinopathy in Parkinson's disease. *Nature Nanotechnology* **13**, 812-818 (2018).
20. I. Kang, J. M. Yoo, D. Kim, J. Kim, M. K. Cho, S.-E. Lee, D. J. Kim, B.-C. Lee, J. Y. Lee, J.-J. Kim, N. Shin, S. W. Choi, Y.-H. Lee, H. S. Ko, S. Shin, B. H. Hong, K.-S. Kang, Graphene Quantum Dots Alleviate Impaired Functions in Niemann-Pick Disease Type C in Vivo. *Nano Letters*, (2021).
21. H. H. Uhlig, F. Powrie, Translating Immunology into Therapeutic Concepts for Inflammatory Bowel Disease. *Annual Review of Immunology* **36**, 755-781 (2018).
22. L. Albenberg, C. M. Brensinger, Q. Wu, E. Gilroy, M. D. Kappelman, R. S. Sandler, J. D. Lewis, A Diet Low in Red and Processed Meat Does Not Reduce Rate of Crohn's Disease Flares. *Gastroenterology* **157**, 128-136.e125 (2019).
23. M. F. Neurath, Cytokines in inflammatory bowel disease. *Nature Reviews Immunology* **14**, 329-342 (2014).

24. K. Machiels, M. Joossens, J. Sabino, V. De Preter, I. Arijs, V. Eeckhaut, V. Ballet, K. Claes, F. Van Immerseel, K. Verbeke, M. Ferrante, J. Verhaegen, P. Rutgeerts, S. Vermeire, A decrease of the butyrate-producing species Roseburia hominis and Faecalibacterium prausnitzii defines dysbiosis in patients with ulcerative colitis. *Gut* **63**, 1275-1283 (2014).
25. J. J. Hansen, R. B. Sartor, Therapeutic Manipulation of the Microbiome in IBD: Current Results and Future Approaches. *Curr Treat Options Gastroenterol* **13**, 105-120 (2015).
26. S. Wang, I. S. Cole, Q. Li, The toxicity of graphene quantum dots. *RSC Advances* **6**, 89867-89878 (2016).
27. R. Kurapati, J. Russier, M. A. Squillaci, E. Treossi, C. Ménard-Moyon, A. E. Del Rio-Castillo, E. Vazquez, P. Samorì, V. Palermo, A. Bianco, Dispersibility-Dependent Biodegradation of Graphene Oxide by Myeloperoxidase. *Small* **11**, 3985-3994 (2015).
28. C. Martín, G. Jun, R. Schurhammer, G. Reina, P. Chen, A. Bianco, C. Ménard-Moyon, Enzymatic Degradation of Graphene Quantum Dots by Human Peroxidases. *Small* **15**, 1905405 (2019).
29. M. A. Dobrovolskaia, S. E. McNeil, Immunological properties of engineered nanomaterials. *Nature Nanotechnology* **2**, 469-478 (2007).
30. W. Zhang, L. Yan, M. Li, R. Zhao, X. Yang, T. Ji, Z. Gu, J. J. Yin, X. Gao, G. Nie, Deciphering the underlying mechanisms of oxidation-state dependent cytotoxicity of graphene oxide on mammalian cells. *Toxicol Lett* **237**, 61-71 (2015).
31. B.-C. Lee, J. Y. Lee, J. Kim, J. M. Yoo, I. Kang, J.-J. Kim, N. Shin, D. J. Kim, S. W. Choi, D. Kim, B. H. Hong, K.-S. Kang, Graphene quantum dots as anti-inflammatory therapy for colitis. *Science Advances* **6**, eaaz2630 (2020).
32. J. Ma, R. Liu, X. Wang, Q. Liu, Y. Chen, R. P. Valle, Y. Y. Zuo, T. Xia, S. Liu, Crucial Role of Lateral Size for Graphene Oxide in Activating Macrophages and Stimulating Pro-inflammatory Responses in Cells and Animals. *ACS Nano* **9**, 10498-10515 (2015).
33. Y. Chong, Y. Ma, H. Shen, X. Tu, X. Zhou, J. Xu, J. Dai, S. Fan, Z. Zhang, The in vitro and in vivo toxicity of graphene quantum dots. *Biomaterials* **35**, 5041-5048 (2014).
34. L. Yu, X. Tian, D. Gao, Y. Lang, X.-X. Zhang, C. Yang, M.-M. Gu, J. Shi, P.-K. Zhou, Z.-F. Shang, Oral administration of hydroxylated-graphene quantum dots induces intestinal injury accompanying the loss of intestinal stem cells and proliferative progenitor cells. *Nanotoxicology* **13**, 1409-1421 (2019).

Chapter 2

Graphene quantum dots as anti-inflammatory therapy for colitis

2.1 Introduction

Intestinal bowel diseases (IBDs) including Crohn's disease and ulcerative colitis are destructive, relapsing tissue disorders that involve dysregulation of the local immune response and compromised intestinal barrier function (*1*). The pathophysiology of IBDs is associated with exaggerated T cell responses (*2*) and related macrophages, which are one of the most abundant myeloid cells in the peritoneal cavity, including intestinal mucosa. The extensive interactions between T cells and macrophages deteriorate inflammation. Therefore, understanding the mechanism of macrophage's regulation on T cell differentiation is essential in developing novel therapeutics for IBDs. Many approaches have been made to find a way to cure IBDs, and alternative therapeutics are in urgent need as the disease prevails throughout the world (*3*). Although the use of immunosuppressive drugs is one of the main treatments (*4*) and methods to increase the drug delivery to lesion have also been developed (*5*), the treatments for IBDs are often accompanied by complications such as infections and malignancies (*6*). Thus, alternative drug with less side effects is still needed. Recent studies have suggested suitable mouse models for Crohn's disease by introducing genetic modifications and particular microorganisms (*7*). Nevertheless, impaired intestinal barrier function and subsequent dysregulated immune response still are considered as a crucial factor for disease onset (*1*). To address this issue, we tried graphene quantum dots (GQDs) as therapeutics in colitis model mice because previous research has shown that graphene derivatives interact with immune cells including macrophages and T cells (*8*).

This chapter is reproduced from: B. –C. Lee†, J.Y. Lee†, J. Kim, J.M. Yoo, I. Kang, J. Kim, N. Shin, D.J. Kim, S.W. Choi, D. Kim, B.H. Hong, K. Kang* B. –C. Lee et al., 2020, *Sci. Adv.* **6** : eaaz2630 ©American Association for the Advancement of Science

Graphene derivatives, especially GQDs, have high biocompatibility and antioxidant effect, so GQDs have been exploited as a potential therapeutic agent for treating inflammatory diseases (*9*). GQDs can scavenge reactive oxygen radicals by delocalizing electron density in the conjugated ring structure; hence, they are able to reduce oxidative stress. Besides, there are abundant anionic functional groups on the edges, in which the property is known to provoke fewer immune responses compared to positively charged nanoparticles (*10*). In addition, previous studies showed the potential uses of graphene materials in vaccines, immunotherapeutics and immunosuppressive agents (*11*). However, there are few reports on graphene material's roles in autoimmune diseases including IBDs.

IBDs have frequently been studied using the dextran sulfate sodium (DSS) colitis animal model due to its simplicity, reproducibility and rapidity (*12*). Notably, the clinical and histological features of DSS-induced animals are very similar to those observed in human patients. DSS disrupts colonic epithelium, leading to the entry of luminal bacteria and antigens into the mucosa and resulting in stimulation of immune cells and secretion of proinflammatory cytokines and chemokines (*13*). Furthermore, a polarized T helper 1 (T_H1) response and proinflammatory macrophages have been reported to aggravate the inflammatory response in DSS colitis model. For these reasons, we used the DSS colitis model to identify the inhibitory effects of GQDs on acute and chronic colitis.

Our previous study showed that GQDs have protective effects on Parkinson's disease by direct interaction with alpha-synuclein fibrils without toxicity and can be excreted by urine (*14*). In this study, we also confirmed the therapeutic effects of GQDs on colitis model mice without any complications. The *ex vivo* and *in vitro* analyses were proceeded to investigate the underlying mechanisms of the therapeutic effects of GQDs, which regulated T cell and macrophage subsets to facilitate the disease recovery. When GQDs were intraperitoneally (i.p.) injected (Fig.

2-1A), GQDs treatment inhibited the loss of body weight (Fig. 2-1B), lowered the disease activity index score (Fig. 2-1C), and prevented shortening of the colon (Fig. 2-1D). The inhibition of intestinal epithelium damage and fibrosis was also verified (Fig. 2-1E), with the decrease of the pro-inflammatory cytokine expressions (Fig. 2-1F). Furthermore, GQDs did not cause significant toxicity to the healthy mice, confirmed from the no significant difference in the body weight (Fig. 2-2A), the amount of water and food consumption (Fig. 2-2B), and the major organ weights (Fig. 2-2C) compared to the PBS-treated group. GQDs accumulated in abdominal fat were gradually reduced and were excreted through urine (Fig. 2-2D and E).

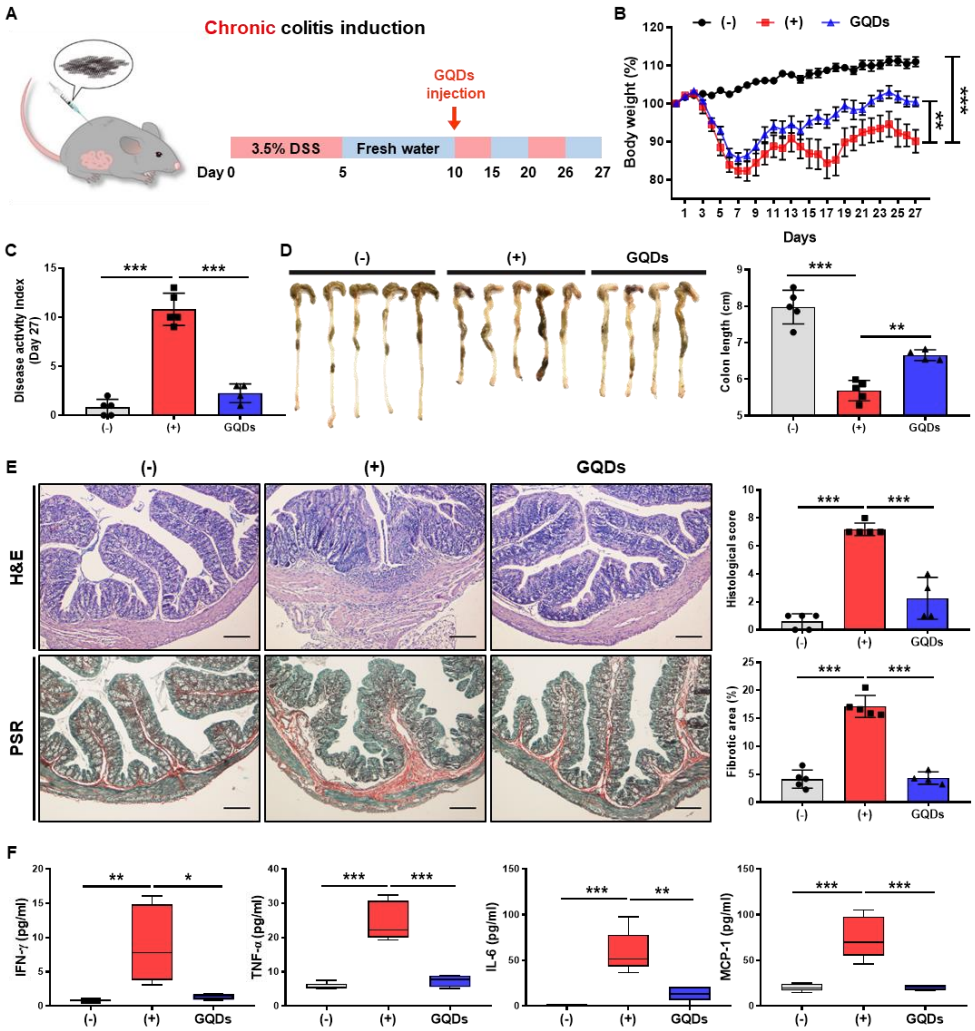

[By Dr. B-.C. Lee, College of Veterinary Medicine, SNU]

Fig. 2-1. Intraperitoneal injection of GQDs effectively alleviates DSS-induced chronic colitis in mice. (**A**) Experimental scheme for DSS-induced chronic colitis and GQDs administration. 3.5% DSS water was repetitively administered to mice to induce colitis. GQDs were injected intraperitoneally (300 μg/head) 10 days after the administration of DSS. **B-F**, Mice received i.p. injections of GQDs after chronic DSS-colitis induction. On day 27, mice were sacrificed for further investigation. (**B**) The percentage of body weight change and (**C**) the DAI for colitis severity was monitored for clinical assessment. (**D**) After 27 days from colitis induction, the lengths of the colons obtained from each group were measured. (**E**) Left: Representative images of colon sections stained with H&E and PSR staining for the assessment of histology and fibrosis. Scale bar=200 μm. Right: Histopathologic evaluations were conducted to examine lymphocyte infiltration and intestinal damage. Quantitative analysis of the fibrotic area (stained in red). (**F**) Serum was collected from the colitis mice, and the secreted levels of the indicated cytokines were assessed using CBA analysis. (*N*=4-5 mice/group). *P<0.05, **P<0.01, ***P<0.001. Results are shown as the mean ± SD. Photo credit: Byung-Chul Lee (Adult Stem Cell Research Center and Research Institute for Veterinary Science, College of Veterinary Medicine, Seoul National University)

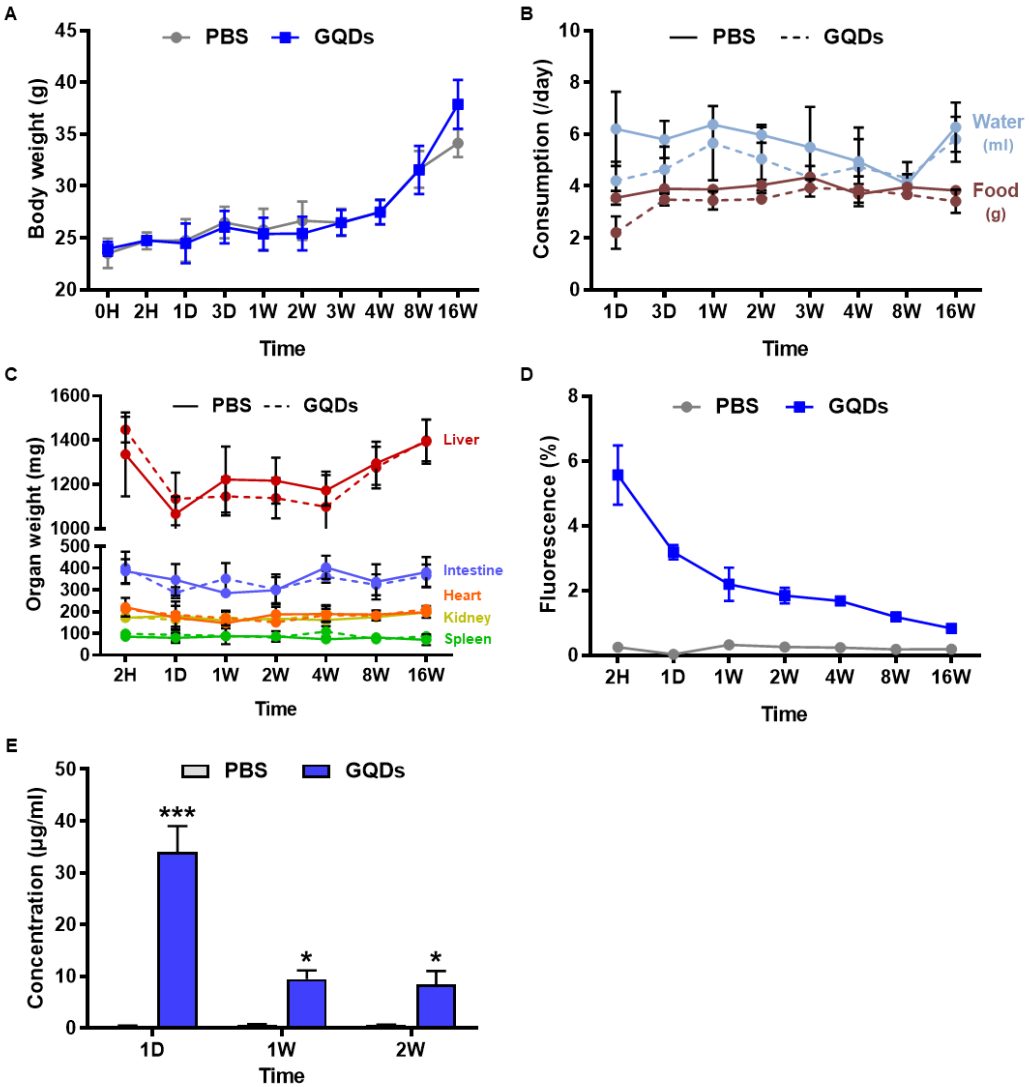

[By Dr. B-.C. Lee, College of Veterinary Medicine, SNU]

Fig. 2-2. GQDs are excreted from mice without generating toxicity. Without DSS induction, biotin-labeled GQDs were injected into normal mice by the same method and dosage and monitored for 16 weeks (*N*=5 mice/group). (**A**) Body weights and (**B**) water and food consumption were measured at each time point. (**C**) Mice were sacrificed at the indicated time points, and organ weights were assessed. (**D**) The FITC-labeled anti-biotin antibody was used to detect the presence of GQDs in the abdominal mesenteric fat. (**E**) Excretion of GQDs was investigated in urine collected from the mice. *P<0.05, **P<0.01, ***P<0.001. Results are shown as the mean ± SD.

2.2 Results

Characterization of GQDs

GQDs were synthesized by the improved Hummer's method according to the previous literature (Fig. 2-3A) (*15*). Transmission electron microscopy (TEM) image showed the lateral size distribution of the GQDs, which had an average size of 28.5 ± 9.7 nm (Fig. 2-3B). The height of the synthesized GQDs was determined by atomic force microscopy (AFM), which showed 7.1 ± 1.8 nm (Fig. 2-3C). The properties of GQDs were further determined by Raman spectroscopy (Fig. 2-3D), exhibiting distinctive D and G bands at 1360 and 1600 cm^{-1}, which are the characteristic peaks of graphene-based materials. GQDs displayed intense and broad D band, which arose from the presence of many defect sites. Functional groups of GQDs were verified by Fourier-transform infrared spectroscopy (FT-IR), elemental analysis (EA), and x-ray photoelectron spectroscopy (XPS). The major peaks from the FT-IR (Fig. 2-3E) spectrum of GQDs were O-H (3430 cm^{-1}), C=O (1730 cm^{-1}), C=C (1620 cm^{-1}), and C-O (1220 cm^{-1}), showing the presence of hydroxyl, carboxyl groups, and epoxide rings. Successful coupling of biotin was proved by the appearance of new peaks at 1400 cm^{-1} (C-H), and at 1080 cm^{-1} (C-O), both derived from polyethylene glycol (PEG). More intense transmittance was observed around 3420 and 1610 cm^{-1} due to the newly formed amide bond. The ratio of oxygen to carbon of GQDs was measured by EA (Table 2-1), and the value 0.73 showed the highly oxidized state of graphite. Through XPS (Fig. 2-3F), the binding energy of C-C (284.50 eV), C-O (286.68 eV), and C=O (288.36 eV) bonds was measured. The C-C bond showed the highest content of 50.54%, and the percentage of C-O and C=O was 38.21% and 11.25%, respectively. The surface charge of GQDs was evaluated by zeta potential, in which the measured value -52.2 ± 6.85 mV showed a highly negatively charged surface and well-dispersed property. On the basis of the measured properties of GQDs, we sought to explore the impact of its therapeutic effects against DSS-induced mice.

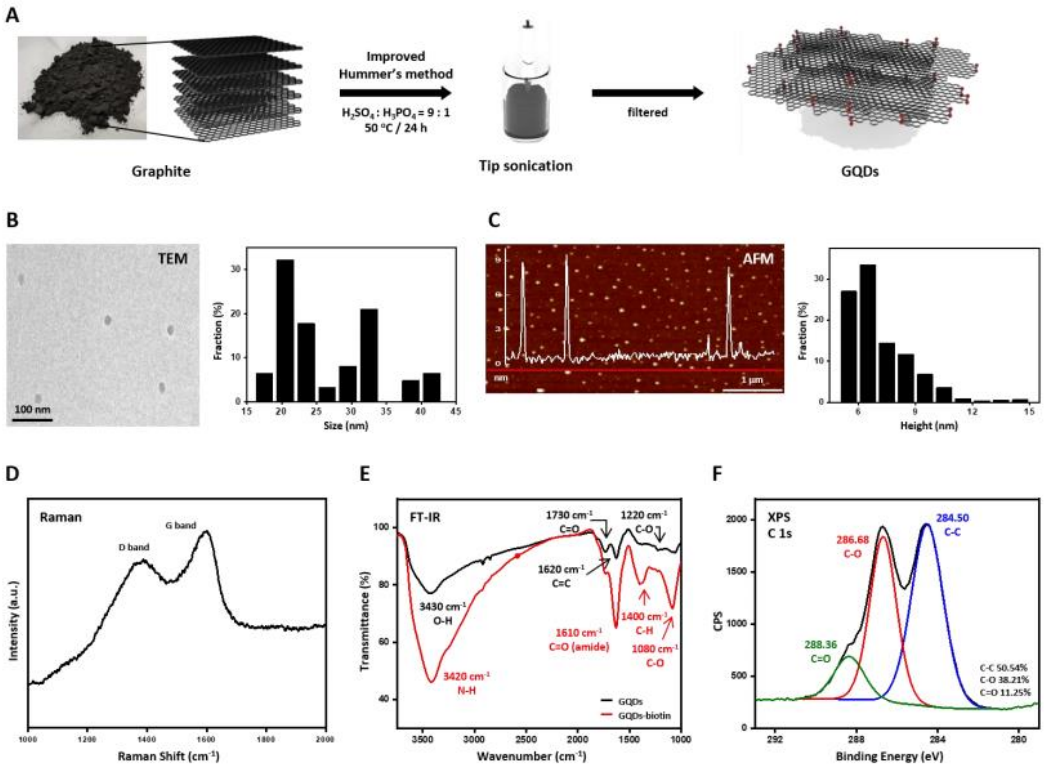

[By Dr. J.M. Yoo, and J. Kim, College of Natural Sciences, SNU, Dr. D.J. Kim, Program in Nano Science and Technology, Graduate School of Convergence Science and Technology, SNU]

Fig. 2-3. Synthesis and characterization of GQDs. (**A**) Schematic representation of the synthesis process for GQDs. (**B**) Representative TEM image of GQDs and the size distribution (n=62). (**C**) Representative AFM image and line profile analysis of GQDs, and the height distribution (n=22). (**D**) Representative Raman spectra of GQDs. (**E**) FT-IR spectra of GQDs and biotin-labeled GQDs. (**F**) XPS spectrum of GQDs, C1s.

Element	wt%	mol%	Molar ratio
C	43.69	42.58	1
H	2.17	25.35	0.60
N	0.00	0.00	0.00
S	2.45	0.90	0.02
O	42.64	31.17	0.73

[By J. Kim, College of Natural Sciences, SNU]

Table 2-1. Elemental Analysis of GQDs

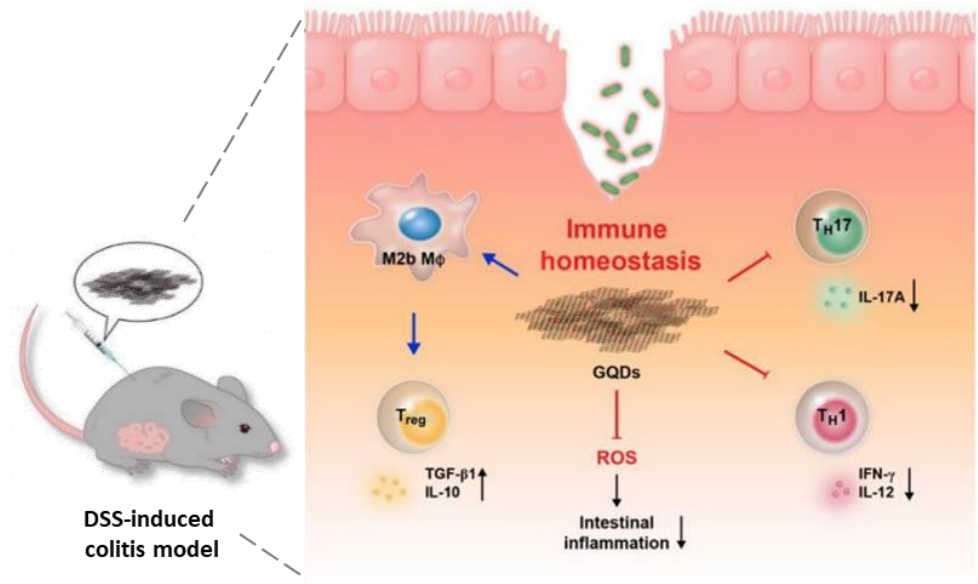

Fig. 2-4. Schematic diagram of the GQDs' effect on colitis.

2.3 Discussion

GQDs recovered intestinal immune homeostasis by suppressing excessive inflammation and facilitating the development of a regulatory loop of T cells (Fig. 2-4). The underlying mechanism of GQDs on immunosuppression is still under research; however, we could interpret the mode of actions based on its structure. As GQDs have a conjugated graphitic domain and abundant hydrogen-donating functional groups on the edges, it is well known for its potent antioxidant effect. Because inflammation is associated with the imbalance between oxidative stress and antioxidants, GQDs' ability to scavenge reactive oxygen species (ROS) can assist in regulating inflammation.

Another factor to consider is that GQDs have a negative surface charge due to carboxyl and hydroxyl groups. The research on the effect of nanoparticle's surface charge on inflammation and immunoregulation has been carried on, and many studies revealed that negatively charged nanoparticles are less prone to provoke immunostimulation (*10*). As the leading treatment target of colitis is to ameliorate

excessive immune responses, injected particles must not induce additional stimulation on the immune system.

Although these findings suggest that the properties of GQDs, including the lateral size, height, and functional groups, are suitable for the use in a clinical application against colitis, it needs to be further investigated whether modifications to GQDs, such as changes to the surface charge, the ratio between functional groups, or addition of a bactericidal effect to the materials, may cause different therapeutic outcomes (*16*).

Despite the fact that GQDs were found in the abdominal cavity, when GQDs are intraperitoneally or intravenously injected, they are distributed through the whole organs and are mainly accumulated in the liver and spleen (*17*). In line with the previous study, we found that injected GQDs preferred to accumulate on greater omentum and mesentery near spleen and colon. Then, the particles are mostly excreted through urine or removed by hepatocytes in the liver through endocytosis (*18*). Also, as GQDs are composed of the hydrophobic graphitic domain and hydrophilic functional groups, and due to their small size, luminal uptake through endocytosis is probable (*19*). Besides the clearance of GQDs through urine, enzymes such as myeloperoxidase and horseradish peroxidase are known to degrade GQDs (*20*). Once they are degraded and become smaller particles, it is much easier to be cleared out through the kidney, as particles smaller than 5 nm are proved to be rapidly excreted through urine (*21*). Therefore, GQDs could be cleared out naturally without generating noticeable toxicity. Nevertheless, validation of the therapeutic efficiency of GQDs via oral administration remains to be determined for actual therapeutic use in practice. With oral administration, the effect of GQDs can be relatively limited to a specific organ, reducing systemic side effects that appeared by any chance.

Overall, intraperitoneally injected GQDs attenuated intestinal inflammation in both acute and chronic DSS-induced experimental colitis models. GQDs

effectively regulated excessive immune responses and prevented tissue damage by indirectly inducing colonic and splenic infiltration of regulatory T cells and converting classical macrophages (M1) to alternative macrophages (M2), particularly the M2b subtype, in the pro-inflammatory milieu. With negligible toxicity and natural clearance, GQDs were able to maintain intestinal immune homeostasis, showing a potency to be utilized in treating IBDs.

2.4 Methods

Preparation of GQDs

First, pristine graphene oxides (GOs) were synthesized through the improved Hummer's method (*15*). To prepare GQDs, the obtained solution of GOs in DI water (3 mg/ml) was vigorously tip-sonicated for 3 hours and vacuum-filtered with cellulose nitrate membrane filter (0.45 μm, GE Healthcare Life Science, Buckinghamshire, UK).

Biotinylation of GQDs

The biotinylation of GQDs was achieved by EDC coupling. First, 10 mg of N-(3-Dimethylaminopropyl)-N`-ethylcarbodiimide hydrochloride, EDC reagent (Sigma, St. Louis, MO, USA) was added to 10 ml of GQDs solution (3 mg/ml) to replace the edge carboxyl groups with EDC reagents. After 30 minutes, 20 mg of Amine-PEG_3-Biotin (Thermo Scientific, San Jose, CA, USA) was subsequently added to the solution to form amide bonds between activated edges of GQDs, and reactive amine groups of biotin for 24 hours. The solution was then dialyzed with a MWCO 1 kD nitrocellulose membrane bag (Fisher Scientific, Hampton, NH, USA) to discard unreacted EDC and biotin molecules. The concentration of the final product was measured by obtaining powder after freeze-drying small amount of the solution.

TEM imaging

The sample solutions (10 μg/ml) were adsorbed to 300 mesh lacey carbon coated copper grids (Ted Pella, Inc., Redding, CA, USA) for 30 mins. The grids were rinsed with a few drops of DI water and thoroughly dried in a desiccator before imaging. The samples were analyzed by a high resolution – transmission electron microscope (HR-TEM, JEM-3010, JEOL Ltd.) and the images were collected by a Gatan Digital Camera (MSC-794) coupled to the microscope.

AFM

The GQDs sample was prepared on a silicon wafer and was measured by XE-100 AFM (Park Systems, Suwon, Republic of Korea) by non-contact mode. The image size of 25 μm^2 was obtained at the scan rate of 0.8 Hz.

Raman spectroscopy

The powder products were prepared on SiO_2 substrates for the Raman spectra measurements. The spectra were obtained by a Renishaw micro-Raman spectrometer with 514.5 nm Ar excitation laser.

FT-IR spectroscopy

Prior to the Fourier-transform infrared spectroscopy (FT-IR) spectra measurements, the powder samples were fully dried in a desiccator to prevent undesirable oxygen containing peaks. The spectra were measured by the conventional KBr pellet method (Nicolet 6700, Thermo Scientific).

Elemental Analysis

The GQDs powder was obtained by freeze-drying the solution, and was kept in a desiccator for more than 3 days to avoid contamination from other elements. The weight percentage of each elements was measured by automatic elemental analyzer (FLASH 2000, Thermo Scientific)

XPS

The GQDs powder was prepared by the same method as for EA. The binding energy of C1s was measured by X-ray photoelectron spectroscopy (AXIS-HSi, KRATOS).

Zeta Potential

The GQDs solution (50 μg/ml) was filtered by 200 nm syringe filter, and the zeta potential was measured by Zetasizer Nano ZS, Malvern.

2.5 References

1. A. Kaser, R. S. Blumberg, The road to Crohn's disease. *Science* **357**, 976-977 (2017).
2. B. Khor, A. Gardet, R. J. Xavier, Genetics and pathogenesis of inflammatory bowel disease. *Nature* **474**, 307 (2011).
3. G. G. Kaplan, The global burden of IBD: from 2015 to 2025. *Nature reviews Gastroenterology & hepatology* **12**, 720-727 (2015).
4. P. S. Dulai, C. A. Siegel, J.-F. Colombel, W. J. Sandborn, L. Peyrin-Biroulet, Systematic review: monotherapy with antitumour necrosis factor α agents versus combination therapy with an immunosuppressive for IBD. *Gut* **63**, 1843-1853 (2014).
5. S. Zhang, J. Ermann, M. D. Succi, A. Zhou, M. J. Hamilton, B. Cao, J. R. Korzenik, J. N. Glickman, P. K. Vemula, L. H. Glimcher, An inflammation-targeting hydrogel for local drug delivery in inflammatory bowel disease. *Science translational medicine* **7**, 300ra128-300ra128 (2015).
6. A. Stallmach, S. Hagel, T. Bruns, Adverse effects of biologics used for treating IBD. *Best practice & research Clinical gastroenterology* **24**, 167-182 (2010).
7. R. Caruso, T. Mathes, E. C. Martens, N. Kamada, A. Nusrat, N. Inohara, G. Núñez, A specific gene-microbe interaction drives the development of Crohn's disease–like colitis in mice *SCIENCE IMMUNOLOGY* **4**, eaaw4341 (2019).
8. M. Feito, M. Vila, M. Matesanz, J. Linares, G. Gonçalves, P. Marques, M. Vallet-Regí, J. Rojo, M. Portolés, In vitro evaluation of graphene oxide nanosheets on immune function. *Journal of colloid and interface science* **432**, 221-228 (2014).
9. V. Volarevic, V. Paunovic, Z. Markovic, B. Simovic Markovic, M. Misirkic-Marjanovic, B. Todorovic-Markovic, S. Bojic, L. Vucicevic, S. Jovanovic, N. Arsenijevic, I. Holclajtner-Antunovic, M. Milosavljevic, M. Dramicanin, T. Kravic-Stevovic, D. Ciric, M. L. Lukic, V. Trajkovic, Large graphene quantum dots alleviate immune-mediated liver damage. *ACS Nano* **8**, 12098-12109 (2014).
10. M. A. Dobrovolskaia, S. E. McNeil, Immunological properties of engineered nanomaterials. *Nature Nanotechnology* **2**, 469-478 (2007).
11. M. Orecchioni, C. Ménard-Moyon, L. G. Delogu, A. Bianco, Graphene and the immune system: Challenges and potentiality. *Advanced Drug Delivery Reviews* **105**, 163-175 (2016).
12. R. Guerrero-Alba, E. E. Valdez-Morales, N. N. Jimenez-Vargas, C. Lopez-Lopez, J. Jaramillo-Polanco, T. Okamoto, Y. Nasser, N. W. Bunnett, A. E. Lomax, S. J. Vanner,

Stress activates pronociceptive endogenous opioid signalling in DRG neurons during chronic colitis. *Gut* **66**, 2121-2131 (2017).

13. M. Perše, A. Cerar, Dextran sodium sulphate colitis mouse model: traps and tricks. *BioMed Research International* **2012**, (2012).
14. D. Kim, J. M. Yoo, H. Hwang, J. Lee, S. H. Lee, S. P. Yun, M. J. Park, M. Lee, S. Choi, S. H. Kwon, S. Lee, S.-H. Kwon, S. Kim, Y. J. Park, M. Kinoshita, Y.-H. Lee, S. Shin, S. R. Paik, S. J. Lee, S. Lee, B. H. Hong, H. S. Ko, Graphene quantum dots prevent α-synucleinopathy in Parkinson's disease. *Nature Nanotechnology* **13**, 812-818 (2018).
15. D. C. Marcano, D. V. Kosynkin, J. M. Berlin, A. Sinitskii, Z. Sun, A. Slesarev, L. B. Alemany, W. Lu, J. M. Tour, Improved synthesis of graphene oxide. *ACS Nano* **4**, 4806-4814 (2010).
16. S. Liu, T. H. Zeng, M. Hofmann, E. Burcombe, J. Wei, R. Jiang, J. Kong, Y. Chen, Antibacterial activity of graphite, graphite oxide, graphene oxide, and reduced graphene oxide: membrane and oxidative stress. *ACS Nano* **5**, 6971-6980 (2011).
17. N. Lu, L. Wang, M. Lv, Z. Tang, C. Fan, Graphene-based nanomaterials in biosystems. *Nano Research* **12**, 247-264 (2019).
18. K. Yang, J. Wan, S. Zhang, Y. Zhang, S.-T. Lee, Z. Liu, In Vivo Pharmacokinetics, Long-Term Biodistribution, and Toxicology of PEGylated Graphene in Mice. *ACS Nano* **5**, 516-522 (2011).
19. H. Zhang, C. Peng, J. Yang, M. Lv, R. Liu, D. He, C. Fan, Q. Huang, Uniform Ultrasmall Graphene Oxide Nanosheets with Low Cytotoxicity and High Cellular Uptake. *ACS Applied Materials and Interfaces* **5**, 1761-1767 (2013).
20. R. Kurapati, J. Russier, M. A. Squillaci, E. Treossi, C. Ménard-Moyon, A. E. Del Rio-Castillo, E. Vazquez, P. Samorì, V. Palermo, A. Bianco, Dispersibility-Dependent Biodegradation of Graphene Oxide by Myeloperoxidase. *Small* **11**, 3985-3994 (2015).
21. M. Nurunnabi, Z. Khatun, K. M. Huh, S. Y. Park, D. Y. Lee, K. J. Cho, Y.-k. Lee, In Vivo Biodistribution and Toxicology of Carboxylated Graphene Quantum Dots. *ACS Nano* **7**, 6858-6867 (2013).

Chapter 3

Oral administration of microbiome-friendly graphene quantum dots as therapy for colitis

3.1 Introduction

Inflammatory bowel diseases (IBDs) comprising ulcerative colitis and Crohn's disease are characterized by gastrointestinal (GI) damage and intermittent intestinal inflammation resulting in disabilities (*1*). The impairment of intestinal barrier function could be triggered by several causes categorized as genetic susceptibility, environmental factors, spontaneous immune response, and abnormal changes in intestinal microbiota (*2*). Undesirable translocation of commensal bacteria through the ruptured intestinal epithelium subsequently activates first line defence cells, macrophages (*3*), dendritic cells (DC) (*4*), and even intestinal epithelial cells (*5*) themselves through innate immune pathways. Antigen presenting cells robustly secrete proinflammatory cytokines including TNF-α, IL-12, and IL-23 to recruit helper T (Th) cells into inflamed sites, while inhibiting the function of regulatory T cells (Tregs), resulting in loss of immune homeostasis. Thus, activated Th1 cells cause excessive immune response during intestinal inflammation by producing their prominent cytokine, IFN-γ. Furthermore, Th17 cells and associated cytokine IL-17 reportedly play an important role in IBD pathogenesis (*6*).

Therefore, the restoration of microbiome balance is an indispensable target of treatment. Although the exact correlation of dysbiosis of the gut microbiome and

---

This chapter is reproduced from: B.-C. Lee†, J.Y. Lee†, J. Kim†, N. Shin, J.M. Yoo, I. Kang, J.-J. Kim, S.-E. Lee, D. Kim, S.W. Choi, B.H. Hong, K.-S. Kang* (Submitted)

pathogenesis is vague, several studies revealed dysbiosis in the DSS-induced colitis model and patients (*7-9*). Though antibiotics, probiotics, and fecal transplantation have been attempted to regulate microbiome, improvements were insignificant or found in certain species (*10, 11*). Anti-inflammatory drugs and immune suppressors are currently being used to alleviate immune responses, yet full recovery has not been achieved with side effects. The difficulty of treatment arises from drug delivery to the lower GI tract due to undesirable degradation or release from the upper track; therefore, enteric coating to protect from gastric acid is essential (*12*).

Graphene-based nanomaterials have attracted attention due to their tunable properties and numerous possible applications. Among them, graphene quantum dots (GQDs) are zero-dimensional nanoparticles consisting of a graphitic domain and oxygen-containing functional groups around the edges. GQDs exhibit great potential for various optoelectronic applications through their size-dependent and edge-sensitive photoluminescence properties (*13*). We have used GQDs to enhance the efficiency of organic photovoltaic cells by balancing light absorptivity and conductivity of active layers (*14, 15*). GQDs were mainly synthesized from graphene oxides (GOs) by chemical exfoliation under a strongly acidic environment. While nitrogen-functionalization or doping can regulate the intrinsic properties of GQDs, it requires further complicated wet-chemical reactions. Thus, we developed a straightforward solvent-free method to prepare nitrogen-doped GQDs (N-GQDs) by directly applying nitrogen plasma to as-grown graphene on Cu (*16*). The resulting N-GQDs could be transferred as a film-like layer or easily dispersed in an organic solvent. We confirmed that the N-GQDs of sizes narrowly distributed around ~5 nm show strong photoluminescence when excited at 365 nm, which makes it useful in the wide range of optoelectronic (*17-19*), photocatalyst (*20*), and energy storage applications (*21-23*).

Furthermore, graphene-based nanomaterials have been applied in the biomedical field. The extent to which toxicity and biocompatibility occur in graphene-based nanomaterials ranges due to varying sizes and surface chemistry (*24*). In terms of sizes, small nGOs less than 40 nm do not cause significant toxicity at moderate concentration and are excreted through the kidney (*25, 26*), while large nGOs cause inflammation (*27*). On the other hand, GQDs, which are less than 20 nm, are quickly cleared out, relative to nGOs, through the kidney and liver (*28*). GQDs have a negative surface charge, and in general, nanoparticles of negative surface charge are less prone to stimulate immune responses and cause toxicity than those with a positive surface charge (*29-31*). Although GQDs are renowned for antioxidant ability, it is still controversial as, in some cases, they instead produce reactive oxygen species (*32*). Therefore, GQDs' toxicity depends on concentration and surface chemistry, and those that are biocompatible have been applied in drug delivery in conjugation with other small molecules (*33*) or photodynamic therapy (*34*). Moreover, with the discovery of the therapeutic efficacy of GQDs, a new field of therapy for incurable diseases opens (*35, 36*).

Applying GQDs with high biocompatibility and anti-oxidant ability, we recently published the protective effect of GQDs on colitis, of which GQDs regulated excessive immune responses and eased symptoms of IBDs (*37*). In the study, GQDs around 20 nm of lateral size were intraperitoneally (i.p) injected into a DSS-induced colitis mice model, and GQDs notably inhibited the development of Th1 cells, the primary source of proinflammatory cytokines. Besides, GQDs restored immune homeostasis through inhibiting polarization of Th17 and inducing infiltration of Tregs. GQDs' effect on macrophages led to the increased polarization toward M2b-specific under the proinflammatory milieu, therefore relieving excess inflammation.

This study aimed to examine whether smaller GQDs, of 2~3 nm, could show a similar effect on colitis when administered orally. We chose smaller GQDs as it

has been proven to be highly biocompatible with negligible toxicity (*35, 36*), and changed the administration route for the ease of treatment and limiting the effect organ-specifically. As GQDs enter the stomach, they are exposed to gastric acid, and whether they can survive and manage to reach the lower intestine was an issue; therefore, its physical and chemical characteristics were analyzed after exposure to HCl. Besides, it turned out that GQDs do not exhibit an antibacterial effect, which GOs are well known for, suggesting GQDs as a microbiome-friendly drug. Herein, we showed a more practical application of GQDs as the treatment for experimental colitis, verifying GQDs can be delivered to the intestine orally and express therapeutic effect.

3.2 Results

3.2.1 Stable physical and chemical properties of GQDs in acidic conditions.

Whether graphene derivatives can activate or suppress immune responses is still controversial due to the complexity in the immune system and the existence of the materials varying on size, oxidation, surface charge, etc (*38, 39*). It has been proved that the nanoparticles with positive surface charge are relatively more toxic (*40*) and cause inflammation (*41*) than the ones with negative surface charge. Therefore, whether the physical and chemical properties of GQDs could change due to the harsh acidic condition of gastric acid was studied.

GQDs used in this study were synthesized by thermo-oxidative cutting of carbon fiber (Fig. 3-1A) (*42*). The lateral size was measured by FE-TEM (Field Emission Transmission Electron Microscope), showing the size of 2.51±0.55 nm (Fig. 3-1B). The thickness was measured by AFM (Atomic Force Microscopy), which is 1.68±0.50 nm (Fig. 3-2A). In order to find out whether GQDs could withstand acidic conditions, GQDs powder was dispersed in HCl solutions at pH2

and pH3 to mimic the gastric acid condition and assessed properties after removing acid through dialysis. From the FE-TEM images, GQDs exposed to pH 2 and 3 solutions had sizes of 2.64±0.71 nm and 2.93±0.73 nm, respectively (Fig. 3-1B). As shown in the magnified inset, the distance between the carbon lattice is approximately 0.3~0.33 nm, showing the non-destructive graphitic domain structure.

The Raman spectrum of pristine GQDs showed a G band and D band, referring to the graphitic domain and the defect sites, respectively (Fig. 3-1C). GQDs exhibit higher G band shift (1590~1600 cm^{-1}) than graphene (~1580 cm^{-1}) due to oxidation and defect sites. The G band's redshift of GQDs exposed to the acidic solution can be explained by the loss of carboxyl groups, leading to the relative increase of the C=C bonds on the graphitic domain (*43*), which was confirmed by FT-IR and XPS (Fig. 3-1D). The D band over G band ratio (I_D/I_G) indicates the extent of defects, and there was no significant difference between GQDs samples, implying no substantial structural disorder in the graphitic domain (*44*). To clarify, an additional freeze-drying process was required to get a powder form of GQDs after dispersion to acid. Therefore, we validated the effect of the extra drying process by dispersing GQDs powder in DI water and re-drying it. As a result, the conserved G and D bands were detected from the re-dried sample (Fig. 3-2B).

As mentioned above, we used FT-IR (Fourier-transform Infrared Spectroscopy) to figure out the types of functional groups in GQDs (Fig. 3-1E). GQDs have abundant hydroxyl (3419 cm^{-1}) and carboxyl groups (1718, 1225 cm^{-1}), with sp^2 carbon domain (1623 cm^{-1}). The carboxyl group (1718 cm^{-1}) and the sp^2 carbon bond transmittance ratio is 1.21, showing the highly oxidized structure. In the case of GQDs dispersed in pH 2 and pH 3 solution, while other peaks were conserved, the decrease in the carboxyl groups' transmittance (~1730 cm^{-1}, ~1250 cm^{-1}) was noticeable. The FT-IR spectrum of the re-dried GQDs also exhibited the reduced transmittance of carboxyl groups (Fig. 3-2C), implying the drying process

contributes to the loss of carboxyl groups. The percentage of each bonding was quantified by XPS (X-ray Photoelectron Spectroscopy) analysis (Fig. 3-1F), where the carboxyl group content of pH2, 3, and re-dried samples decreased (Fig. 3-2D).

Besides, we measured the Zeta potential of each sample as the surface charge affects immune response and toxicity. The surface charge of pristine GQDs was -13.7±4.90 mV, exhibiting a negative charge due to the oxygen-containing functional groups. The surface charge of GQDs dispersed in HCl solutions increased due to protonation (*45*), which was -0.59±3.93 mV, and -5.43±11.1 mV for pH2 and pH3 solution, respectively, yet maintaining net negative charges.

Finally, we conjugated biotin to the carboxyl groups of GQDs to verify the cellular uptake of GQDs. The carboxyl group was activated by EDC reagent, and amine-PEG-linked biotin was attached. The characteristic Raman peaks of GQDs were maintained after the conjugation process (Fig. 3-2E). The successful reaction was confirmed through FT-IR (Fig. 3-2F) by the decrease of transmittance in the carboxyl group (1731, 1241 cm-1) and newly formed C-H (1382 cm-1) and C-O (1089 cm-1) peak.

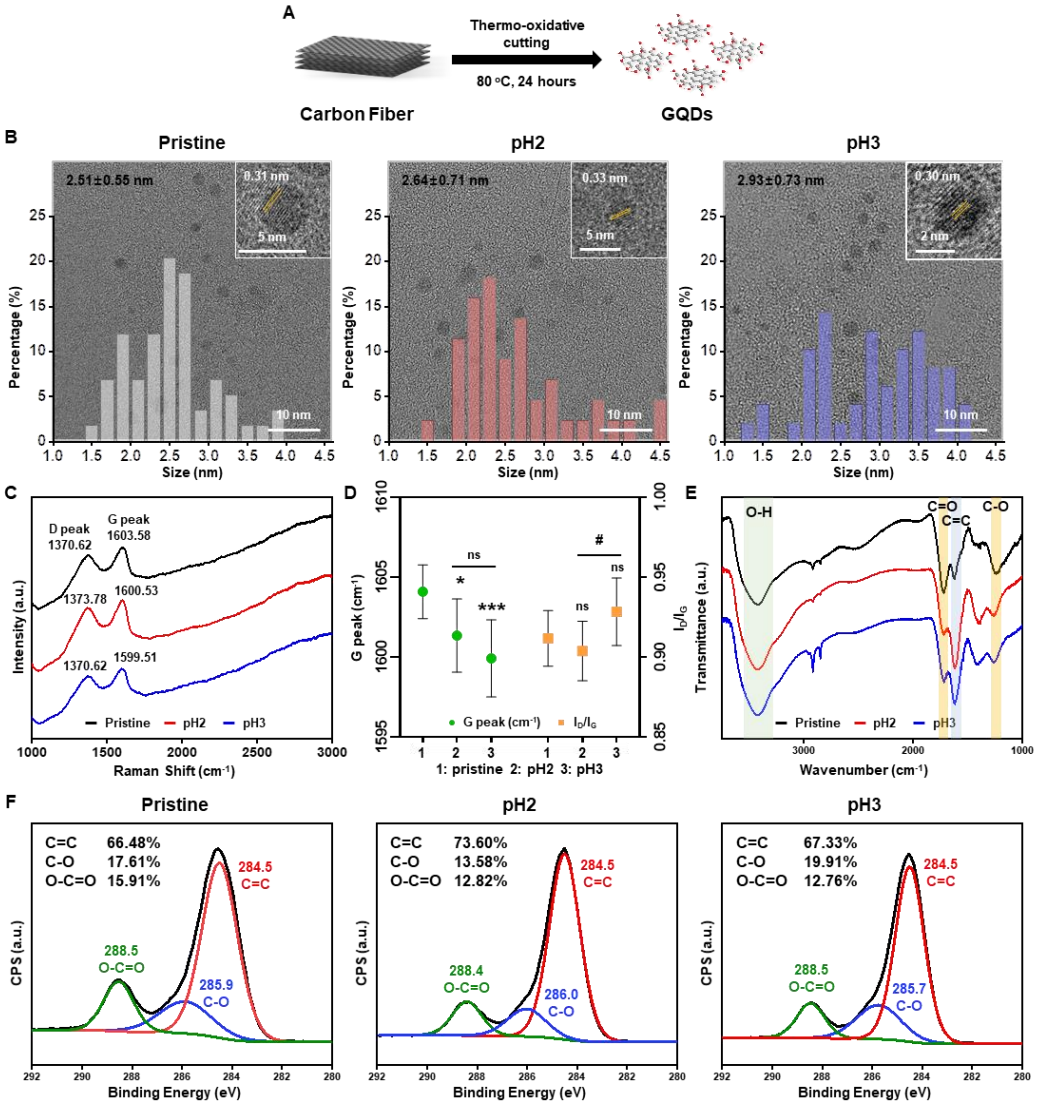

[By J. Kim, College of Natural Sciences, SNU]

Fig. 3-1. Synthesis and physicochemical characteristics of GQDs after acid exposure. (**A**) GQDs are synthesized through the thermo-oxidative cutting of carbon fiber with strong acids. (**B**) Representative FE-TEM images and the size distribution of pristine GQDs, and GQDs treated with HCl solutions of pH 2 and 3. Graphitic lattice is visible in the inset. (pristine GQDs: N=59, pH 2-GQDs: N=44, pH 3-GQDs: N=49) (**C**) Representative Raman spectra of pristine GQDs and GQDs resuspended in HCl solutions. (**D**) The Raman shift of G peak and I_D/I_G value of GQDs at each condition. (N=10 for each group). (**E**) The FT-IR spectra and (**F**) the XPS spectra of pristine GQDs, GQDs treated by pH2, and pH3 HCl solution. Results are shown as the mean ± SD. *P<0.05, **P<0.01, ***P<0.001; DI vs. pH 2 or pH 3. #P<0.05; pH2 vs. pH 3.

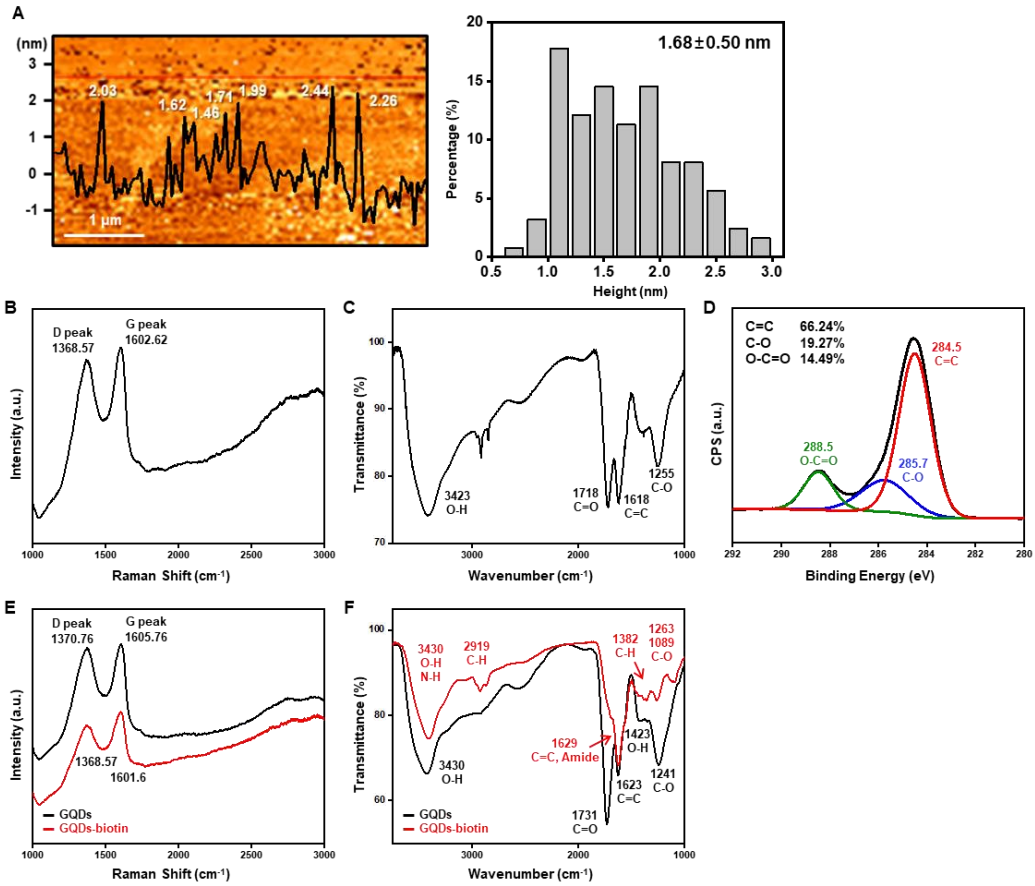

[By J. Kim, College of Natural Sciences, SNU]

Fig. 3-2. Characterization of GQDs. (**A**) The representative AFM image and the height distribution of pristine GQDs. (N=124) (**B**) The Raman, (**C**) the FT-IR, and (**D**) the XPS spectrum of re-dried GQDs. (**E**) The Raman and (**F**) the FT-IR spectra of pristine GQDs and biotin-conjugated GQDs.

3.2.2 Orally administered GQDs suppress degeneration on the DSS-induced colitis mouse model.

Although graphene-derived material's behaviors and biological effects after inhalation and intravenous injection into mice have been actively investigated, the oral feeding effects of GQDs in disease model still remain unclear (*46, 47*). We previously confirmed the therapeutic roles of i.p. injected GQDs on colitis-induced mice (*37*). Given the results from i.p injection experiments with smaller GQDs (Fig. 3-3), we next tried oral administration of GQDs to assess suppressive effects on the acute colitis mouse model. After the induction of colitis, 300 μg of GQDs (1 mg/ml, 300 μl/injection) were orally administered every 3 days (Fig. 3-4A), and after 11 days, we assessed the severity of colitis based on body weights, disease activity index (DAI), and colon length. GQDs protected mice from the loss of bodyweights induced by colitis and relieved disease severity measured by DAI scores (Fig. 3-4B and C). Consistent with the relieved symptoms, we observed a decrease in the shortening of the colon length which is one of the hall marks of experimental colitis (Fig. 3-4D). Therefore, we confirmed that orally delivered GQDs could also ameliorate the DSS-induced colitis similar to i.p injection.

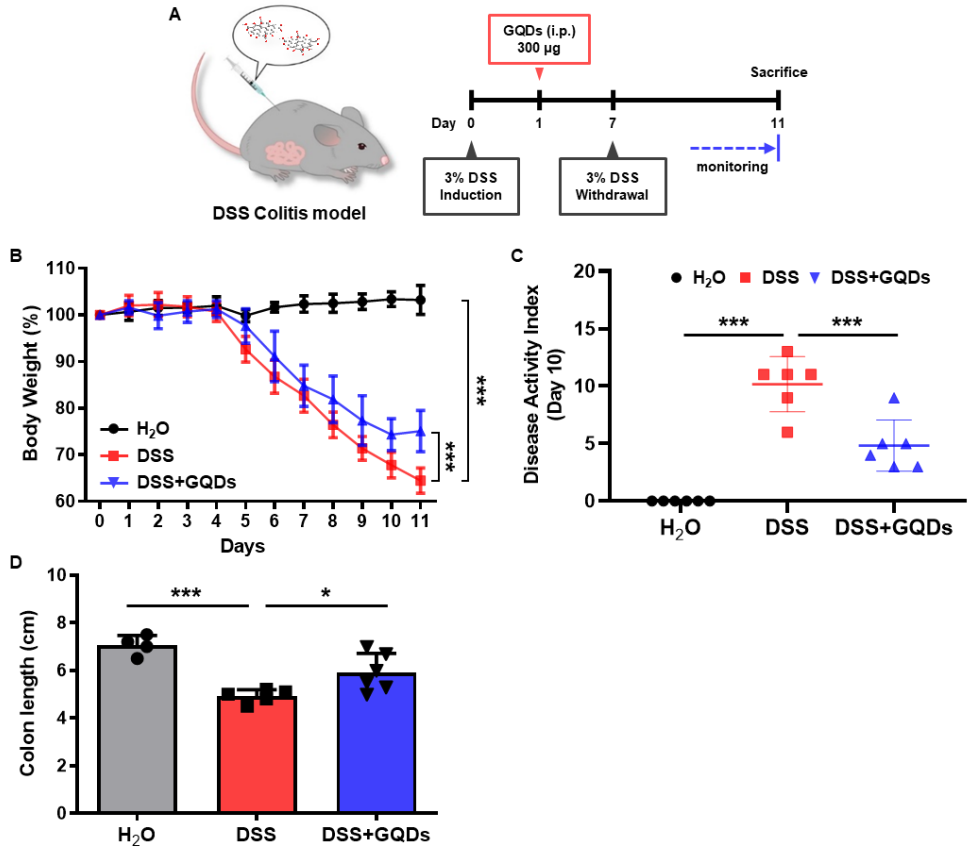

[By Dr. B-.C. Lee, College of Veterinary Medicine, SNU]

Fig. 3-3. Intraperitoneal injection of GQDs suppress DSS-induced colitis in mice. (**A**) Mice were fed with 3% DSS in drinking water for 7 days and GQDs were administered intraperitoneally to the mice on day 1. (**B**) Body weights were monitored until the end of the experiments. (**C**) DAI was assessed on day 10. (**D**) At the end of the experiment, mice were sacrificed and colon's length was measured. (N=4-5 mice/group). *P<0.05, ***P<0.001. Results are shown as the mean ± SD.

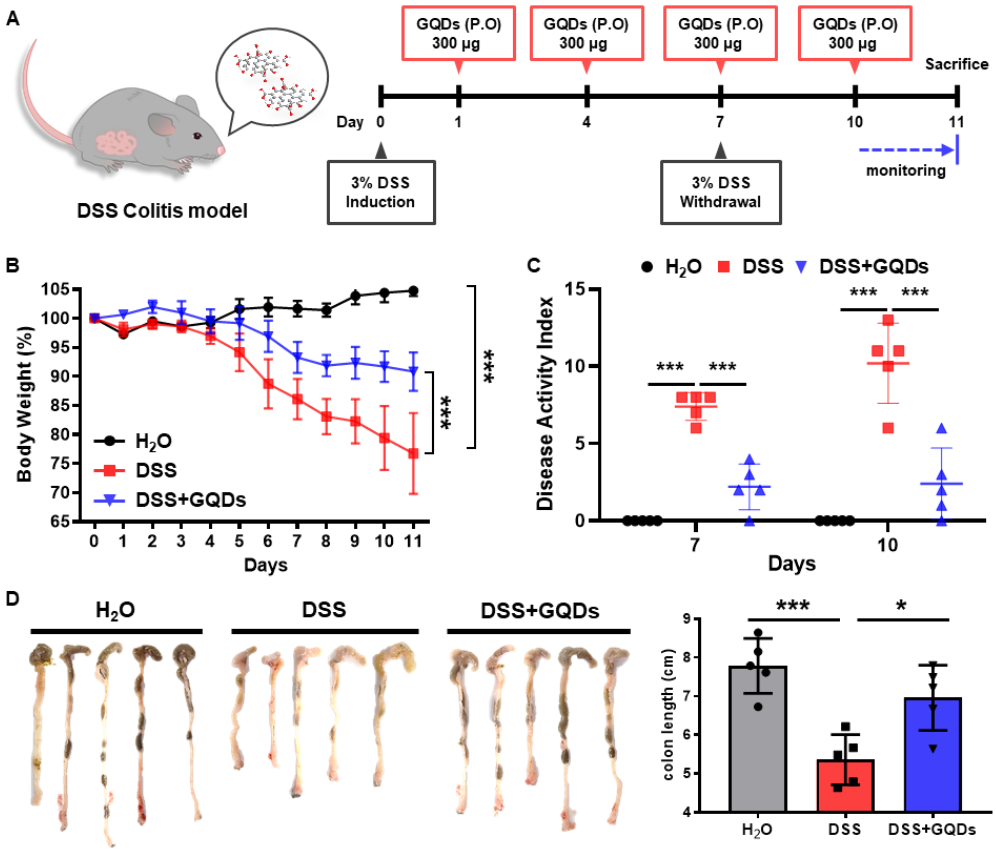

[By Dr. B-.C. Lee, College of Veterinary Medicine, SNU]

Fig. 3-4. Oral administration of GQDs alleviates DSS-induced colitis. (**A**) Mice were fed with 3% DSS in drinking water for 7 days and GQDs were orally administered to the mice on the indicated days (1 mg/ml, 300 μl/injection). (**B**) Body weights were measured every day. (**C**) Disease severity was determined under criteria of DAI on day 7 and 10. (**D**) On day 11, mice were sacrificed and colon's lengths were measured. (N=5 mice/group). *P<0.05, ***P<0.001. Results are shown as the mean ± SD. Photo credit: Byung-Chul Lee (Adult Stem Cell Research Center and Research Institute for Veterinary Science, College of Veterinary Medicine, Seoul National University)

3.2.3 Orally administered GQDs mitigate intestinal inflammation and tissue damage.

We sought to investigate whether orally administered GQDs have anti-inflammatory effects in the colitis-induced mice. Histologic analyses of colons showed that GQDs attenuated the destruction of crypts and decreased neutrophil infiltration (Fig. 3-5A). GQD treatment protected colon from a loss of crypts caused by DSS-induced colitis. Due to inflammatory cell infiltration, submucosa showed significant edema in DSS group. GQD treatment significantly decreased the edema and immune cell infiltration. GQDs also reduced excessive collagen deposition and fibrosis in the colons, reflecting decreased colonic inflammation (Fig. 3-5B). We then addressed the suppressive effect of GQDs on systemic inflammation in colitis-induced mice by detecting the level of pro-inflammatory cytokines in the serum of mice. Consistent with decreased intestinal pathology, pro-inflammatory cytokines, including IL-6, TNF-α, MCP-1, and IL-12, were attenuated in GQDs treated mice (Fig. 3-5C), and displayed decreased splenomegaly compared with control mice (Fig. 3-6A). This data suggests that orally delivered GQDs can effectively inhibit colonic inflammation and damage induced by DSS.

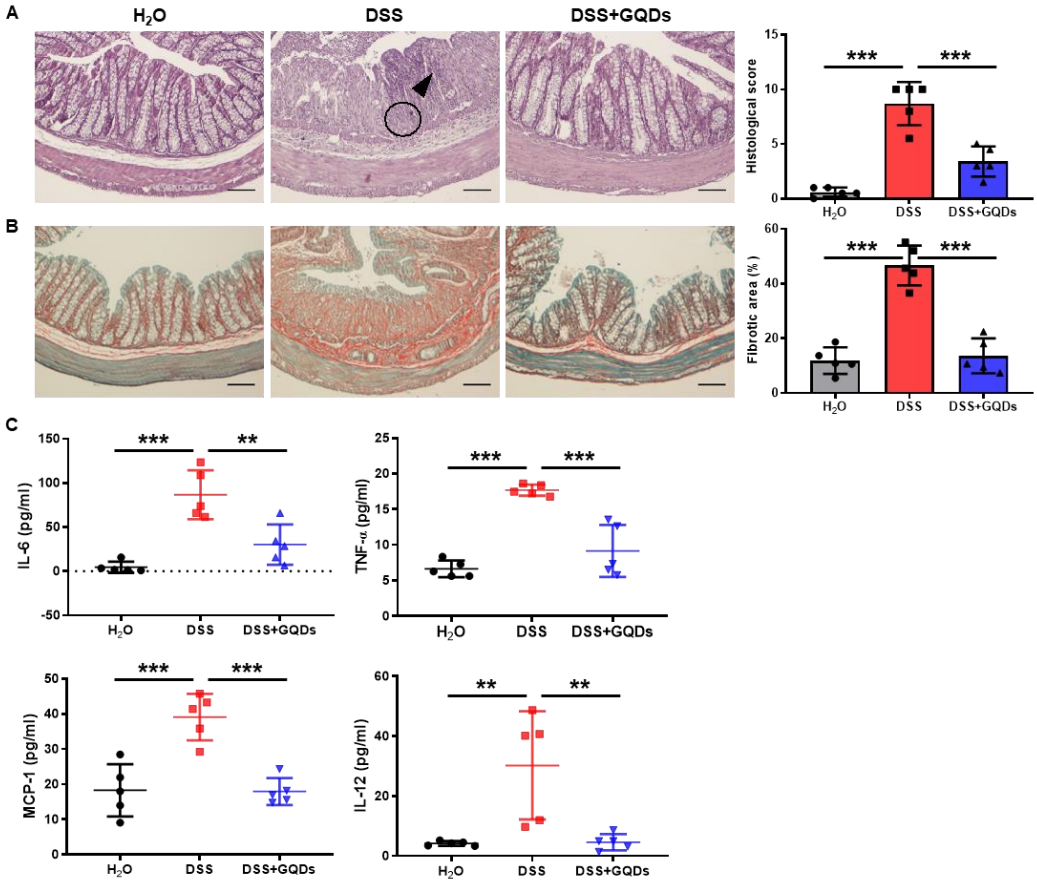

[By Dr. B-.C. Lee, College of Veterinary Medicine, SNU]

Fig. 3-5. Effects of GQDs on colonic inflammation and inflammatory cytokines in serum. (**A**) Representative images of H&E-stained colons (left) and histological scores of colons measuring lymphocyte infiltration and intestinal damage (right). A loss of crypts (arrow) and neutrophil infiltration (circle) can be seen. Scale bar=200 μm. (**B**) Representative images of picro-sirius red (PSR) stained colons (left) and quantification of fibrotic regions (Right). Scale bar=200 μm. (**C**) The levels of pro-inflammatory cytokines were measured in mice serum. (N=5 mice/group). **P<0.01, ***P<0.001. Results are shown as the mean ± SD. Photo credit: Byung-Chul Lee (Adult Stem Cell Research Center and Research Institute for Veterinary Science, College of Veterinary Medicine, Seoul National University)

3.2.4 GQDs modulate immune cell composition by intracellular infiltration.

The decreased spleen's size after administration of GQDs to DSS-induced mice suggests that GQDs can suppress systemic inflammatory responses (Fig. 3-6A). To assess the direct effects of GQDs on immune cells, we treated GQDs in primarily cultured immune cells. GQDs suppressed proliferation of concanavalin A-activated human mononuclear cells (hMNCs) dose-dependently (Fig. 3-6B). Among hMNCs, the percentages of T cells (CD3, CD4, CD8), macrophages (CD14), and myeloid cells (CD33) were compromised in response to GQDs treatments (Fig. 3-6C), which indicates the suppressive effect of GQDs on inflammation by directly inhibiting external stimuli-dependent proliferation of immune cells.

Next, the inhibitory effects of GQDs on T cells and macrophage differentiation were examined. First, we observed cytoplasmic location of GQDs using biotin-conjugated GQDs in cultured $CD4^+$ T cells (Fig. 3-7A). Interestingly, GQDs inhibited the proliferation of $CD4^+$ T cells (Fig. 3-7B), and the treatment of GQDs on Th1 differentiated T cells decreased the excretion of Th1 responsive cytokines (Fig. 3-7C). Furthermore, GQDs increased the Treg population within hMNC pool (Fig. 3-7D) and directly accelerated differentiation of Tregs implying a resolution of excessive inflammation in the colitis model (Fig. 3-7E). In addition, GQDs suppressed the activity of pro-inflammatory M1 macrophages, which contribute to colitis development. As shown in T cells, GQDs were also detected in the cytoplasm of macrophages (Fig. 3-8A). GQDs inhibited M1 polarized macrophage's proliferation (Fig. 3-8B) and decreased M1 macrophage-specific genes (Fig. 3-8C). In addition, GQDs significantly suppressed phagocytosis, which represents functional features of classically activated M1 macrophages (Fig. 3-8D and E). These results demonstrate that GQDs relieved intestinal inflammation by direct regulation of pro-inflammatory immune cells.

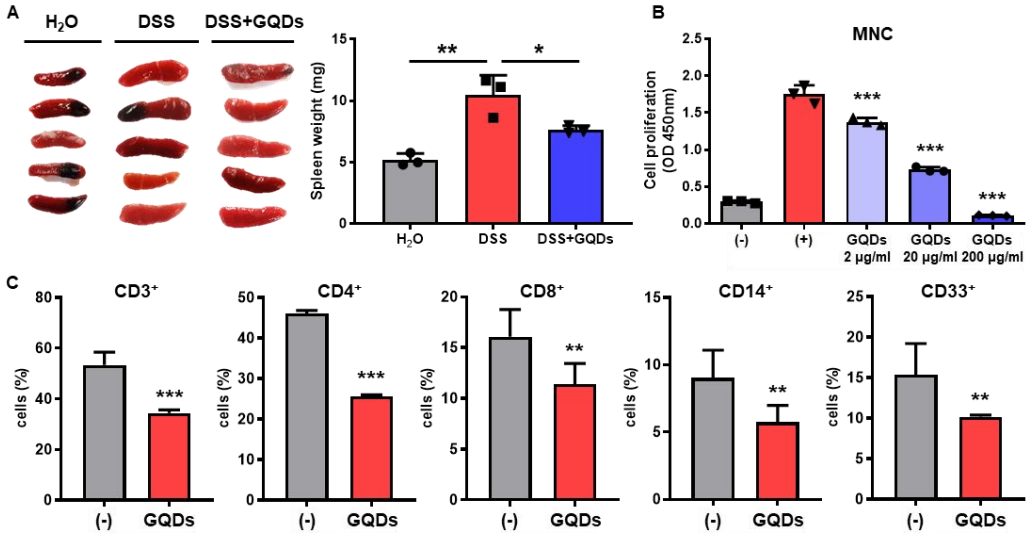

[By Dr. B-.C. Lee, College of Veterinary Medicine, SNU]

Fig. 3-6. GQDs suppress immune cell activity. (**A**) Images of spleens from mice (right) and spleen weights (left). (N=4-5 mice/group). (**B**) Proliferation of hMNCs and (**C**) frequency of each immune cells were measured in hMNCs after treatments of GQDs (20 μg/ml). *P<0.05, **P<0.01, ***P<0.001. Results are shown as the mean ± SD. Photo credit: Byung-Chul Lee (Adult Stem Cell Research Center and Research Institute for Veterinary Science, College of Veterinary Medicine, Seoul National University)

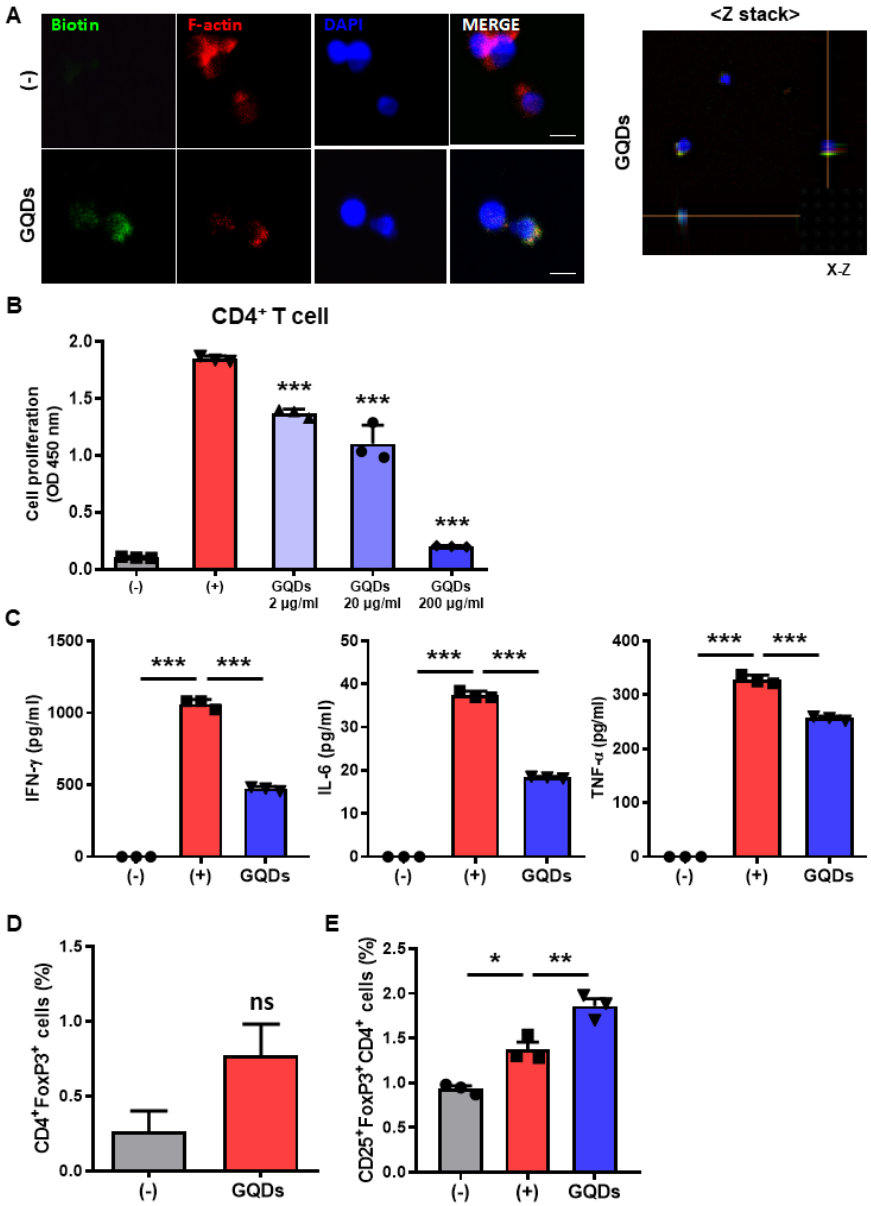

[By Dr. B-.C. Lee, College of Veterinary Medicine, SNU]

Fig. 3-7. GQDs have an effect on the CD4⁺ T cells. CD4⁺ T cells from hMNCs were differentiated in vitro under Th1 or Treg-promoting conditions with GQDs. (**A**) After biotin-conjugated GQDs treatment (20 μg/ml) for 2 days, GQDs were detected using GFP-anti biotin antibody for the localization. F-actin was stained to show a contour of the cell. Right: Z-stack image of GQDs treated CD4⁺ T cells. Scale bar=5 μm. (**B**) CD4⁺ T cell's proliferation was measured using BrdU assay kit. (**C**) Levels of IFN-γ, IL-6 and TNF-α were analyzed in the supernatant of cultured cells. (**D**) To assess effects of GQDs on regulatory T cell's emergence, CD4⁺FoxP3⁺ cell's population was analyzed using flow cytometry in hMNCs. (**E**) Regulatory T cells were polarized and the proportion of CD4⁺CD25⁺FoxP3⁺ cells were determined by flow cytometry. *P<0.05, **P<0.01, ***P<0.001. Results are shown as the mean ± SD.

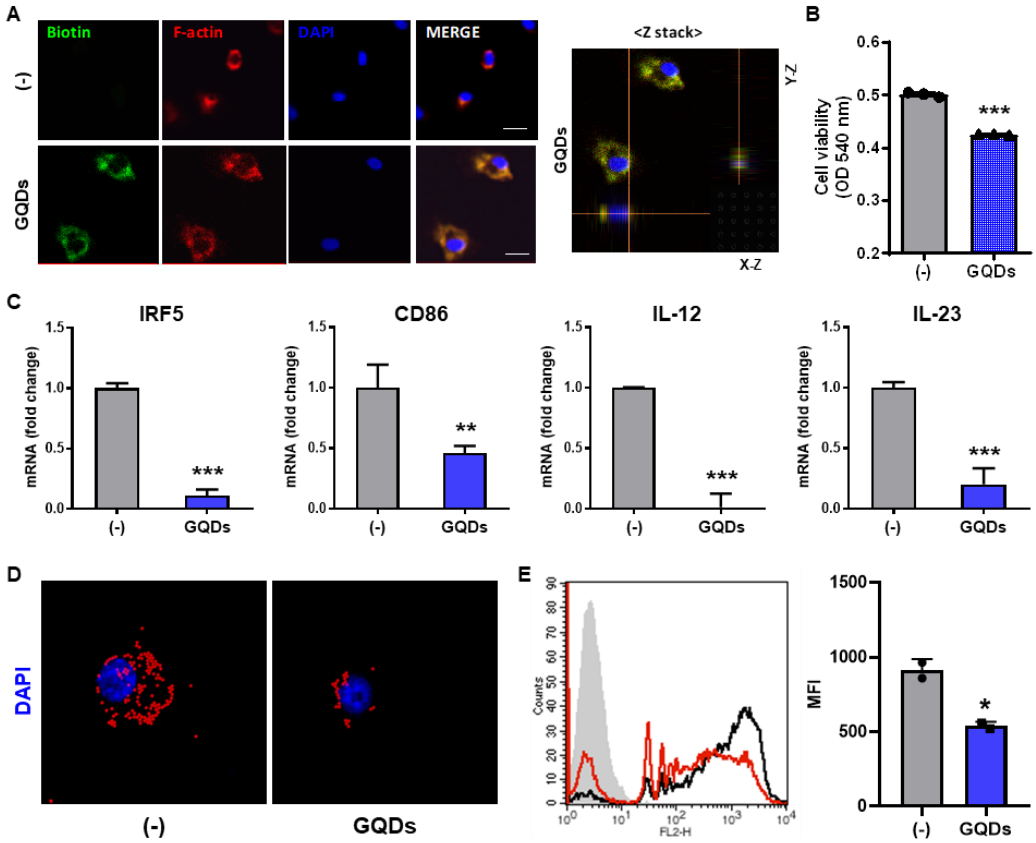

[By Dr. B-.C. Lee, College of Veterinary Medicine, SNU]

Fig. 3-8. GQDs suppress M1 macrophage's activity. A-D, $CD14^{+}$ cells were isolated from hMNCs and differentiated into M1 macrophages using IFN-γ (20 ng/ml) and LPS (1 μg/ml) with treatment of GQDs (20 μg/ml). (**A**) After biotin-conjugated GQD treatments, GQDs were detected using GFP-anti biotin antibody for the localization. F-actin was stained to show a contour of the cell. Right: Z-stack image of GQDs treated macrophages. Scale bar=5 μm. (**B**) Cell viability was measured using CCK-8. (**C**) Indicated pro-inflammatory cytokine expressions were measured by quantitative PCR. **D-E**, Phagocytic activities of macrophages were assessed using latex beads. (**D**) Representative images. (**E**) Mean fluorescence intensity. *P<0.05, ***P<0.001.

3.2.5 Orally infused GQDs does not show any harmful effect.

To test inflammatory effects in normal state, we delivered GQDs orally in the normal mice and assessed the level of inflammatory cytokines in serum (Fig. 3-9A). Most of pro-inflammatory cytokines were not increased or suppressed in response to GQDs delivery suggesting lack of immune toxicity. In addition, we also measured the number of proliferating cells in the intestinal epithelial cells using Ki67 (Fig. 3-9B). GQDs didn't affect the proliferation of intestinal cells implying that GQDs alleviated colitis by suppressing excessive inflammatory responses in the intestine. Evaluation of the GQD's effect on microbiota was critical as large GOs are known as antibacterial, and beneficial bacteria must have been preserved. In comparison with GQDs, we prepared GOs synthesized by the improved Hummer's method (*48*). GOs have a broad size distribution of 4.50±2.93 μm (Fig. 3-10A). From the FT-IR spectrum, the hydroxyl (3421, 1383 cm^{-1}) and carboxyl groups (1736 cm^{-1}) with C=C bonds (1624 cm^{-1}) and epoxide C-O (1223, 1053 cm^{-1}) were found (Fig. 3-10B). When GQDs of various dosages were treated to BL21 E. Coli and monitored colony formation, no significant bacterial toxicity was found (Fig. 3-9C and D). However, when GOs were co-incubated, the number of colonies decreased notably at 0.1 mg/ml (Fig. 3-9E and F). Taken together, oral administration of GQDs do not cause harmful effect in intestinal cells and gut microbiota.

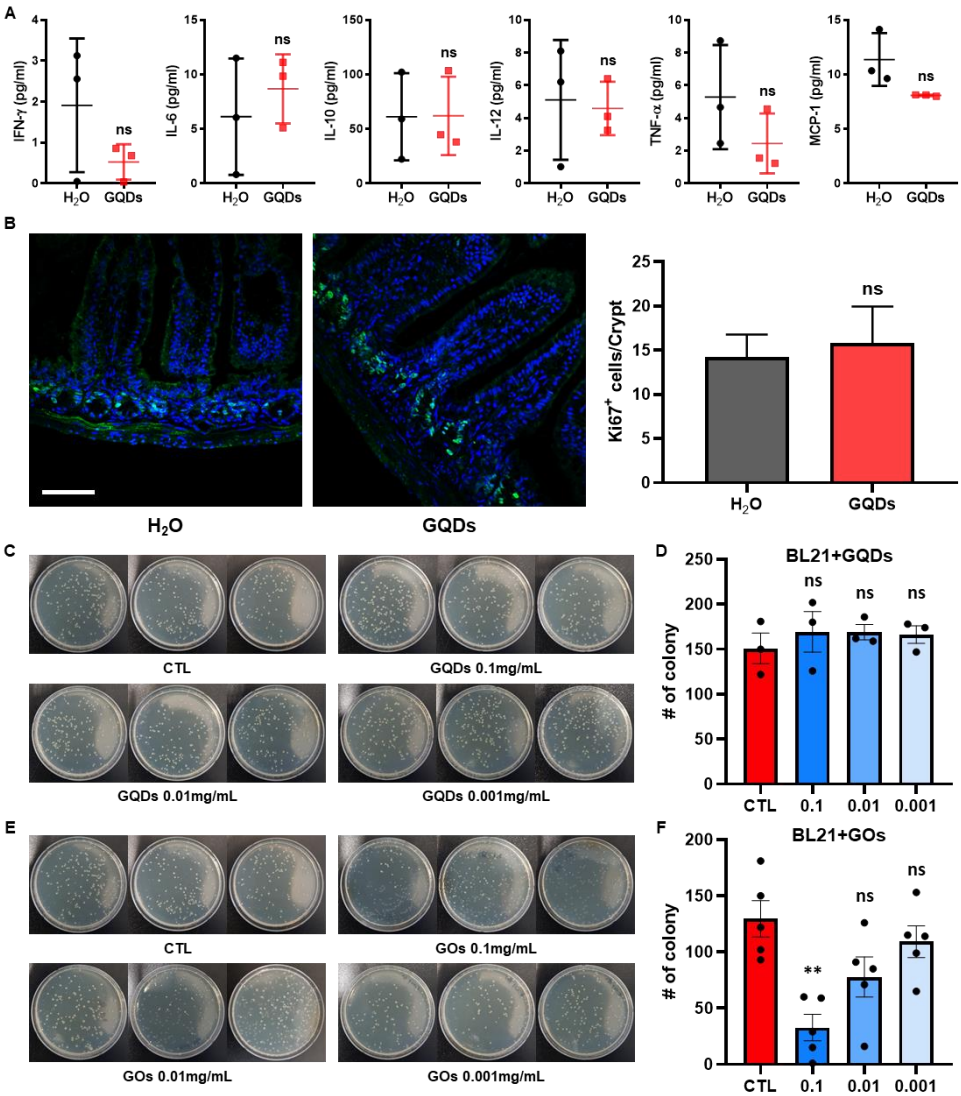

[A-B, By Dr. B-.C. Lee, College of Veterinary Medicine, SNU / C-F, By Dr. D. Kim, Biographene Inc.]

Fig. 3-9. Oral administration of GQDs does not exert toxic effects. A-B, Mice were orally injected with GQDs (1 mg/ml, 300 μl/injection) and sacrificed after 24 hours of injection. Blood and intestine samples were collected at the time of sacrifice. (**A**) The levels of cytokines were measured in mice serum. (**B**) Representative images of Ki67-stained upper intestinal part (left) and quantification of Ki67 expressing cells/crypt (right). Scale bar=100 μm. (**C**) Representative image of the BL21 colony after GQDs treatment. (**D**) Compared to the control group, when GQDs were treated at 0.001 to 0.1 mg/ml, no significant decrease in the number of colonies was found. (**E**) Representative image of the BL21 colony after GOs treatment. (**F**) A significant decrease in the number of colonies was observed due to the high toxicity of GOs. (N=3 mice/group). *P<0.05, **P<0.01, ***P<0.001. Results are shown as the mean ± SD. Photo credit: (**B**) Byung-Chul Lee (Adult Stem Cell Research Center and Research Institute for Veterinary Science, College of Veterinary Medicine, Seoul National University), (**C, E**) Donghoon Kim (Biographene Inc.)

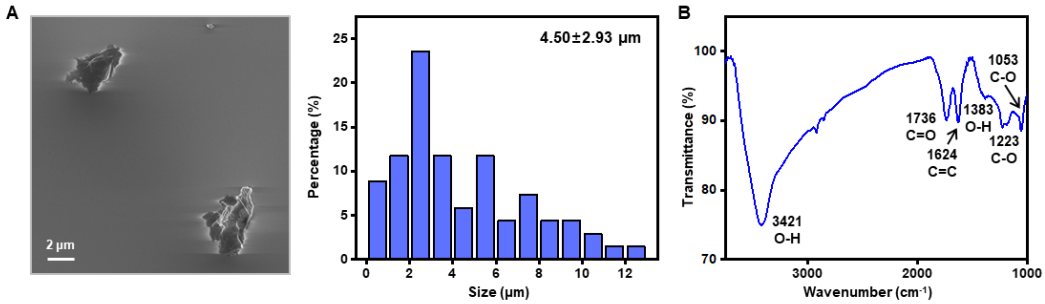

[By J. Kim, College of Natural Sciences, SNU]

Fig. 3-10. Characterization of GOs. (**A**) The representative FE-SEM image and the size distribution of GOs. (N=68) (**B**) The FT-IR spectrum of GOs.

3.3 Discussion

Graphene-based nanomaterials have been widely applied in inflammatory diseases; however, its immunomodulatory functions by oral delivery have not been fully assessed (*49, 50*). Herein, we investigated the anti-inflammatory effects of orally administered GQDs on the DSS-induced colitis model, showing the potential of GQDs as an edible treatment in chronic colitis by relieving intestinal inflammation.

In the present study, we showed that oral administration of GQDs alleviated disease severity in experimental colitis model by partially restoring body weight and physiological signs. Consistent with those phenotypes, we detected significant resolution of intestinal inflammation and fibrotic tissue degeneration in histologic assessment after oral delivery of GQDs similar to our previous study using i.p. injection such as infiltration of neutrophils and hyperemia. In this study, we set the same amount of GQDs for single delivery and delivered the materials repetitively considering presumable rapid wash out than i.p injection. Fortunately, we achieved meaningful outcomes with initial setting, and for this reason, no additional optimization process was performed. Orally delivered GQDs suppressed the expression of pro-inflammatory genes by restraining T cell activation and viability of primarily cultured macrophages, consistent with validation from THP-1 macrophage cell line (*51*). As micro-sized GOs significantly increased the secretion of inflammatory cytokines in macrophages (*52*), and transient increase of the cytokine levels was found from the previous study (*37*), GQDs' smaller size can be responsible for restraining excess inflammation. Furthermore, GQDs treatment inhibited phagocytosis of M1 macrophage, examined by the reduced uptake of microbeads. This implies a suppressed pro-inflammatory property of macrophages, suggesting GQDs as a macrophage modulator regulating inflammatory responses. Future studies can be done with regulatory pathways in macrophages, involving phagocytosis reduction and the release of pro-inflammatory cytokines. Intracellular

or pericellular location of GQDs in macrophages or T cells can be investigated to determine GQDs and immune cells' exact interaction mechanism.

Oral administration is one of the ideal ways of drug delivery due to its simplicity, convenience, and durability, especially in controlling chronic diseases (*53*). However, orally delivered materials can lose their activity in digestion by biological obstacles such as an acidic environment in the stomach, resident time of the drug, and bacterial population in the GI tract. Therefore, several materials, including graphene and carbon nanotubes, were assessed for protection to enhance drug delivery efficiency (*54*). As GQDs were synthesized at harsh acidic conditions, GQDs used in this study did not show significant physical and chemical property changes when exposed to stomach acid-like conditions. The characteristic Raman peaks were preserved, with no significant difference in the I_D/I_G value. The acidic environment formed by HCl would not cause a significant effect on carboxyl groups. Under acidic conditions, carboxyl groups are protonated and able to form hydrogen bonding with the chloride ions (*55*). As dialysis proceeds and the pH rises, chloride ions will be desorbed, and deprotonation would follow, revealing the anionic carboxyl group. Continuous exposure to various ions in water during dialysis and freeze-drying conditions could have led to carboxyl groups' loss. For example, decarboxylation of salicylic acid is available by various metal cation-involved benzoate salts catalysts (*56*). Despite the additional experimental procedures, yet GQDs maintained the oxidized structure. While few-layer graphene and GOs were unstable in low pH environments, which exhibited a positive Zeta potential value (*57*), GQDs' surface charge maintained a negative value in pH2 and 3 solutions, implying a possible immunosuppressive effect.

Although graphene-based nanomaterials showed a therapeutic effect in diverse disease models (*35, 58*), enhancement in efficacy has been made by surface modification (*59-61*) or conjugating to cytokine DNAs (*49, 61*). In some cases, surface modification is required as large-sized GOs are known to cause oxidative

stress. However, our previous and current results showed GQDs' therapeutic efficacies against colitis without adjustments due to their negligible toxicity. In addition to this, adequate clearance is needed for therapeutic applications. In our previous study, we employed i.p. injection route and observed an accumulation of GQDs near the intestinal tissues (*37*). Although we were not able to detect any toxic effect, some researcher elucidated that large size of graphene derivates cause a toxic effect in the body or individual cells (*62*). Orally administered GOs have been reported to be excreted completely within a week (*63*). Thus, we assumed that oral administration of GQDs would take an advantage of rapid wash out in the aspect of accumulation and its possible toxic effect. However, GQDs were not found in either urine or feces after one day of administration, which could be due to degradation by natural enzymes such as horseradish peroxidase and myeloperoxidase (*64*), fast digestion, or difficult detection due to dilution.

Considering the safety issue by oral delivery, Yu et al. have recently reported that daily oral injection of hydroxylated GQDs caused intestinal injury by oxidative stress and apoptosis in intestinal epithelial cells and intestinal stem cells (*65*). The effect of orally administered GOs on dysbiosis has been studied in zebrafish (*66*) and the hyperlipidemic mouse model (*67*), where GOs caused dysbiosis by increasing or decreasing specific strains of bacteria such as *Lactobacillus* and *Clostridium*. Although we administered GQDs orally more often than the previous i.p. injection method, GQDs did not cause immune toxicity or affect the intestinal epithelial cells' proliferation. Furthermore, GQDs exhibited no effect in the proliferation of commensal bacteria when treated during the bacterial culture, suggesting the promising potential of GQDs as a microbiome-friendly nano-drug. Moreover, by adopting a smaller size of GQDs than previous ones (*37*), it is expected that the risk of potential toxicity(*62*) can be further reduced.

In conclusion, orally administered GQDs relieved excessive inflammation in the DSS-induced colitis model without causing side effects. GQDs were able to survive harsh acidic conditions similar to the stomach, preserving its physicochemical properties. Furthermore, the negligible toxicity of GQDs toward bacteria potentiates GQDs as alternative therapeutics in inflammatory diseases through oral administration.

3.4 Methods

Synthesis of GQDs

GQDs were synthesized by the previously reported method (*42*). Briefly, carbon fiber was cut into small pieces and mixed with the sulfuric acid and nitric acid solution of volume ration 3:1. The reaction was carried on at 80 ºC for 24h, with vigorous stirring. After dilution, acid was removed through dialysis (MWCO (Molecular Weight Cut-Off) 1 kD nitrocellulose membrane bag, Thermo Fisher Scientific, USA) and vacuum-filtered, using 100 nm and 20 nm anodisc filter in a row (AnosicTM 47, Whatman, GE Healthcare Life Sciences, Germany). The solvent was removed through the rotary evaporator, and freeze-dried to obtain a powder. The final product was kept in a desiccator and resuspended for later use.

GQDs-biotinylation

GQDs were suspended in the MES buffer (BupH™ MES Buffered Saline Packs, Thermo Fisher Scientific, USA), and EDC (N-(3-Dimethylaminopropyl)-N′-ethylcarbodiimide hydrochloride, Sigma-Aldrich, USA), was added to activate carboxyl groups. After 20 mins of stirring, NH_3-PEG_3-biotin (EZ-Link™, Thermo Fisher Scientific, USA) was added to react with the activated carboxyl groups on GQDs. After the reaction, the solution was dialyzed to remove unreacted species and freeze-dried to obtain GQDs-biotin powder.

Synthesis of GOs and FE-SEM (Field Emission Scanning Electron Microscope) analysis

GOs were synthesized by the improved Hummer's method (*48*). Graphite powder (M14A028, Alfa Aesar, USA) and potassium permanganate were mixed with the sulfuric acid and phosphoric acid of 9:1 volume ratio and stirred at 50 ^{o}C for 24 h. After complete cooling, hydrogen peroxide was slowly added and diluted with DI water. Multiple cleaning was done by a centrifuge to remove acid and freeze-dried to obtain a powder. Then, the GOs solution was spin-coated on a silicon wafer and dried multiple times. The images were taken by FE-SEM (SUPRA 55VP, Carl Zeiss, Germany) and used ImageJ software 1.52a (US National Institutes of Health, USA) for size analysis.

GQDs stability in HCl solution

The solution of pH1 and pH2 was made by using HCl (Hydrochloric acid, ACS reagent, 37%, Sigma-Aldrich, USA). GQDs of 5 mg/ml was mixed with the HCl solution so that the final concentration is 1 mg/ml and pH to become 2 or 3. The mixture was stirred for 2 hours and dialyzed to remove the acid. The solutions were then freeze-dried to obtain a powder.

FE-TEM (Field Emission Transmission Electron Microscope)

GQDs were suspended in water at a concentration of 2 μg/ml. Before usage, the TEM grid (Lacey Carbon, 300 mesh, Cu, 01895-F, TedPella, USA) was coated with graphene, and the GQDs solution was dropped on the grid and air-dried. The images were taken by FE-TEM (JEM-F200 (TFEG) (JEOL Ltd, Japan), with CCD Camera (OneView camera, Gatan, USA), and the size was measured by ImageJ software 1.52a (US National Institutes of Health, USA).

Raman Spectroscopy

GQD samples for Raman spectroscopy were prepared as same as AFM samples. For

the verification of GQDs in various tissues, the tissues were ground with tip-sonication, and after 200 nm syringe filtering, the solution was drop-casted on the Si wafer. All the spectra were obtained by Raman spectrometer (Micro-Raman spectrometer, Renishaw, UK) using a 514 nm laser.

FT-IR (Fourier-transform Infrared Spectroscopy)

GQDs and GOs powder was used to make a KBr pellet, and the spectra were measured by the FT-IR spectrometer (Nicolet 6700, Thermo Scientific, USA).

XPS (X-ray Photoelectron Spectroscopy)

The GQDs powder was coated on the Cu tape, and the binding energy was measured by XPS (AXIS-HSi, KRATOS, UK), and the spectra were deconvoluted using Casa XPS program (Casa Software Ltd., UK).

AFM (Atomic Force Microscopy)

GQDs solution was spin-coated on a silicon wafer and dried multiple times. The area of 10x10 μm^2 was measured by AFM (Park Systems, Republic of Korea) through non-contact mode.

Zeta Potential

The pristine GQDs dispersed in DI water, pH2 and pH3 HCl solutions were prepred at the final concentration of 50 ug/ml. Each solution was filtered with a 0.20 μm syringe filter, and the zeta potential was measured by Zetasizer Nano ZS (Malvern Instruments Ltd, Malvern, UK).

GQDs and GOs toxicity to bacteria

GQDs and GOs concentration of 0.001, 0.01, and 0.1 mg/ml were treated to BL21 and incubated at 37 ^oC for 6 hours. The bacteria were spread on an LB agar plate (Thermo Fisher Scientific, USA) and kept overnight and counted the number of

colonies.

DSS-induced colitis and GQD administration

For acute colitis, 6-week old C57BL/6 mice (Orientbio, Sungnam, Republic of Korea) received 3% (w/v) DSS in drinking water for 7 days. 300 μl of GQDs (1 mg/ml) were orally (4 times, once every 3 days) or intraperitoneally (single) administered to mice at indicated days (figure 2(a)). Body weights were monitored daily and the disease activity index (DAI) was measured by evaluation of body weight loss, activity, stool consistency, bleeding and hair condition at day 7 and 10. Mice were sacrificed for further ex vivo assessments. All animal studies were carried out in accordance with the approved guidelines of Seoul National University Institutional Animal Care and Use Committee (IACUC No. SNU-170523-4).

Histological assessment

Colon samples were fixed in 10% formalin for 24 hours and were processed into dehydration with ethanol, clearing with xylene and wax infiltration with paraffin. Paraffin-embedded blocks were cut into 5-μm sections and stained with hematoxylin and eosin (H&E) and picrosirius red (PSR). H&E stained colon sections were scored by symptomatic criteria including loss of goblet cells, hyperemia/edema, infiltration of immune cells, the presence of crypt abscesses and loss of epithelium. The area of fibrotic tissue was measured in PSR stained sections by picrosirius red and quantified using ImageJ software version 1.46r (US National Institutes of Health, USA).

Immunohistochemistry

To determine the toxicity on intestinal regeneration, upper intestinal part samples were obtained from mice a day after GQD oral administration. The samples were processed as described above and the paraffin slides were deparaffinized and then blocked with 5% normal goat serum solution. The sections were incubated with Ki67 antibody (Abcam, Cambridge, MA, USA) for 12 hours. Then, the sections were

incubated with secondary antibody, Alexa Fluor 488 (Invitrogen) followed by DAPI staining. Images were captured using a confocal microscope (Eclipse TE200, Nikon, Japan).

Cytokine secretion measurements

IFN-γ, TNF-α, IL-6, MCP-1, IL-10 and IL-12 levels in cell culture supernatant and mouse serum were measured using a Cytometric Bead Array (CBA) kit for mouse inflammation (BD Biosciences, San Jose, CA, USA) according to manufacturer's instruction. The CBA kit for Th1/Th2/Th17 (BD Bioscience) was used to evaluate cytokine secretion of the primary cells in vitro. The results were detected using flow cytometer.

Isolation and culture of hMNCs

Isolation of hMNC was conducted as previously described (*68*). Briefly, the blood samples were mixed with HetaSep solution (Stem cell Technologies, Vancouver, Canada) at a ratio of 5:1 and placed at room temperature for one hour. After the incubation, supernatant layer was collected and carefully layered upon Ficoll avoiding intermingling of the two phases. Mononuclear cells were acquired using density gradient centrifugation (2,500 rpm for 20mins). The acquired cells were washed twice in PBS and used for further experiments. All experimental procedures involving human umbilical cord blood or UCB-derived cells were carried out in accordance with the approved guidelines of the Boramae Hospital Institutional Review Board (IRB) and the Seoul National University IRB (IRB No.1707/001-008).

Cell proliferation assay

To assess the proliferation of the cells, the cell proliferation ELISA kit (Roche, Indianapolis, IN, USA) was used according to the manufacturer's instructions. The cells were incubated with 100 μM of BrdU-labeling reagent for 2 hours at 37°C in a humidified atmosphere with 5% CO2. After 30 minutes of fixation with the FixDenat

solution, the cells were incubated in anti-BrdU antibody solution for 90 minutes and subsequently incubated in the provided substrate (tetramethyl-benzidine; TMB) solution for 5 to 30 minutes at room temperature. The level of cell proliferation was quantified by measuring the absorbance at wavelengths of 450 nm and 690 nm (as a reference).

Isolation and Polarization of T cells

Naïve $CD4^+$ T cells were separated from freshly isolated hUCB-MNCs with the human Naïve $CD4^+$ T cell isolation kit II (Miltenyi Biotec, Bergisch Gladbach, Germany) according to the manufacturer's instruction. Naïve $CD4^+$ T cells were cultured in RPMI1640 (Gibco BRL, Grand Island, NY, USA) supplemented with 10% of Fetal Bovine Serum (FBS), anti-CD3/28 bead activator and 20 ng/ml of IL-2, which were essential for the proliferation of the T cell subsets. To differentiate the cells toward T cell subtypes, type-specific cytokines were added to the growth media (20 ng/ml of IFN-γ and 20 ng/ml of IL-12 for type-1 helper T cells and 20 ng/ml of TGF-β1 for Treg cells) and cultured for 5 days at 37 °C in a humidified atmosphere with 5% CO_2 in the presence/absence of GQDs. Polarized Th1 and Treg cells were verified with type-specific staining and flow cytometry. For Th1 cells, surface staining with CD4 antibody followed by intracellular staining for IFN-γ, CD4, CD25 and FoxP3 antibodies was carried out for the Treg analysis.

Isolation and Polarization of Macrophages

Macrophages were separated from freshly isolated hUCB-MNCs with the human $CD14^+$ monocyte-like cells isolation kit (Miltenyi Biotec, Bergisch Gladbach, Germany) according to the manufacturer's instructions. $CD14^+$ monocyte-like cells were cultured in RPMI1640 (Gibco BRL, Grand Island, NY, USA) supplemented with 10% Fetal Bovine Serum (FBS) and stabilized for 2 days with GM-CSF for M1. 20 ng/ml of IFN-γ and 1 μg/ml of LPS were added to the growth media and cultured for 5 days at 37°C in a humidified atmosphere with 5% CO_2 in the presence/absence

of GQDs.

Flow cytometric analysis

Cell surface molecules including CD3, CD4, CD8, CD14, CD25 and CD33 were stained in PBS with 0.5% BSA. Intracellular staining was performed after surface staining to detect FoxP. Data were collected with FACS Calibur (BD bioscience, San Jose, CA, USA) and results were analyzed with FlowJo software (FlowJo, LLC, Ashland, OR, USA).

RNA isolation and Quantitative PCR

Total RNAs were isolated with TRIzol (Invitrogen, Carlsbad, CA, USA) according to the manufacturer's instructions. cDNAs were prepared with SuperScript III Reverse Transcriptase (Invitrogen). Quantitative PCR was performed on an ABI 7300 detection system (Applied Biosystems, Foster City, USA) using SYBR Green PCR Master Mix. The measurement of each gene expression was repetitively conducted 3 times. Detailed sequence for primers were described in Table 3-1.

Gene	Species	Forward	Reverse
IRF5	human	TGCGGACTGATGTGGAGATG	CTGACCAGACCAGAGACAGC
CD86	human	AGGCAACAATGAGCAGACCA	ACTATGGCTTGTTGGGTGGG
IL-12	human	ACCGTAAGTGTCTGGAAGGC	TCTGTCTGCTTCTCACAGGG
IL-23	human	AAATCTACCACCCCAGGCAC	AATCCTCCCCAAACTGTCCC
GAPDH	human	AAGGACACTGAGCAAGAGAGG	GTATTCAAGAGAGTAGGGAGGGC

[By Dr. B-.C. Lee, College of Veterinary Medicine, SNU]

Table 3-1. Quantitative RT-PCR primers

Phagocytosis assay

Primary $CD14^+$ monocyte/macrophage cells were isolated from hMNCs using human $CD14^+$ monocyte-like cells isolation kit (Miltenyi Biotec, Bergisch Gladbach, Germany). The cells were stabilized in the presence of GM-CSF and subsequently polarized with M1 type-specific trophic factors, 20 ng/ml of IFN-γ and 1 μg/ml of LPS for 5 days. Then, the cells were incubated in the media containing red fluorescent microbeads, FluoroSpheres (Thermo Fisher scientific, USA) for 2 hours.

After the incubation, phagocytic activity was determined by flow cytometer or confocal microscopy.

Immunofluorescence analysis

Cells were fixed with 4% paraformaldehyde (PFA) in PBS for 15 minutes at room temperature, and then permeabilized with 0.25% Triton X-100 (Sigma) for 10 minutes. The fixed cells were incubated with blocking solution (5% normal goat serum) for 1 hour at room temperature and incubated with primary antibodies overnight at 4°C. The cells were incubated with secondary antibodies labeled with Alexa Fluor 594 (Invitrogen). DAPI (Sigma) staining was conducted for 5 minutes for the nuclei.

Statistical analysis

The results are expressed as the mean ± SD. Statistical analyses were conducted using Student's 3-tailed t-test or one-way ANOVA followed by the Bonferroni post-hoc test for multi-group comparisons using GraphPad Prism version 8.0 (GraphPad Software, San Diego, CA, USA). Statistical significance is indicated in the figure legends.

3.5 References

1. C. Lu, B. Baraty, H. Lee Robertson, A. Filyk, H. Shen, T. Fung, K. Novak, C. Ma, R. Panaccione, J. P. Achkar, Systematic review: medical therapy for fibrostenosing Crohn's disease. *Aliment. Pharmacol. Ther.*, (2020).
2. I. C. Roberts-Thomson, R. V. Bryant, S. P. Costello, Uncovering the cause of ulcerative colitis. *JGH Open* **3**, 274-276 (2019).
3. E. Meroni, N. Stakenborg, M. F. Viola, G. E. Boeckxstaens, Intestinal macrophages and their interaction with the enteric nervous system in health and inflammatory bowel disease. *Acta Physiologica* **225**, e13163 (2019).
4. D. Bernardo, M. Chaparro, J. P. Gisbert, Human intestinal dendritic cells in inflammatory bowel diseases. *Mol. Nutr. Food Res.* **62**, 1700931 (2018).
5. M. Z. Cader, A. Kaser, Recent advances in inflammatory bowel disease: mucosal immune cells in intestinal inflammation. *Gut* **62**, 1653-1664 (2013).
6. M. Friedrich, M. Pohin, F. Powrie, Cytokine networks in the pathophysiology of inflammatory bowel disease. *Immunity* **50**, 992-1006 (2019).
7. S. Liu, W. Zhao, P. Lan, X. Mou, The microbiome in inflammatory bowel diseases: from pathogenesis to therapy. *Protein Cell*, (2020).
8. P. M. Munyaka, M. F. Rabbi, E. Khafipour, J.-E. Ghia, Acute dextran sulfate sodium (DSS)-induced colitis promotes gut microbial dysbiosis in mice. *J. Basic Microbiol.* **56**, 986-998 (2016).
9. K. Machiels, M. Joossens, J. Sabino, V. De Preter, I. Arijs, V. Eeckhaut, V. Ballet, K. Claes, F. Van Immerseel, K. Verbeke, M. Ferrante, J. Verhaegen, P. Rutgeerts, S. Vermeire, A decrease of the butyrate-producing species Roseburia hominis and Faecalibacterium prausnitzii defines dysbiosis in patients with ulcerative colitis. *Gut* **63**, 1275-1283 (2014).
10. J. J. Hansen, R. B. Sartor, Therapeutic Manipulation of the Microbiome in IBD: Current Results and Future Approaches. *Curr. Treat. Options Gastroenterol.* **13**, 105-120 (2015).
11. R. B. Sartor, G. D. Wu, Roles for Intestinal Bacteria, Viruses, and Fungi in Pathogenesis of Inflammatory Bowel Diseases and Therapeutic Approaches. *Gastroenterology* **152**, 327-339.e324 (2017).
12. A. K. Philip, B. Philip, Colon targeted drug delivery systems: a review on primary and novel approaches. *Oman Med J* **25**, 79-87 (2010).
13. S. Kim, S. W. Hwang, M.-K. Kim, D. Y. Shin, D. H. Shin, C. O. Kim, S. B. Yang, J. H. Park, E. Hwang, S.-H. Choi, G. Ko, S. Sim, C. Sone, H. J. Choi, S. Bae, B. H. Hong, Anomalous Behaviors of Visible Luminescence from Graphene Quantum Dots: Interplay between Size and Shape. *ACS Nano* **6**, 8203-8208 (2012).
14. J. K. Kim, M. J. Park, S. J. Kim, D. H. Wang, S. P. Cho, S. Bae, J. H. Park, B. H. Hong, Balancing Light Absorptivity and Carrier Conductivity of Graphene Quantum Dots for High-Efficiency Bulk Heterojunction Solar Cells. *ACS Nano* **7**, 7207-7212 (2013).
15. D. H. Wang, J. K. Kim, S. Jin Kim, B. Hee Hong, J. H. Park, Efficient solution-processed small-molecule solar cells by insertion of graphene quantum dots. *Nanoscale* **6**, 15175-15180 (2014).
16. J. Moon, J. An, U. Sim, S.-P. Cho, J. H. Kang, C. Chung, J.-H. Seo, J. Lee, K. T.

Nam, B. H. Hong, One-Step Synthesis of N-doped Graphene Quantum Sheets from Monolayer Graphene by Nitrogen Plasma. *Adv. Mater.* **26**, 3501-3505 (2014).
17. J. K. Kim, S. J. Kim, M. J. Park, S. Bae, S.-P. Cho, Q. G. Du, D. H. Wang, J. H. Park, B. H. Hong, Surface-Engineered Graphene Quantum Dots Incorporated into Polymer Layers for High Performance Organic Photovoltaics. *Sci. Rep.* **5**, 14276 (2015).
18. K. D. Lee, M. J. Park, D.-Y. Kim, S. M. Kim, B. Kang, S. Kim, H. Kim, H.-S. Lee, Y. Kang, S. S. Yoon, B. H. Hong, D. Kim, Graphene Quantum Dot Layers with Energy-Down-Shift Effect on Crystalline-Silicon Solar Cells. *ACS Applied Materials & Interfaces* **7**, 19043-19049 (2015).
19. J. Kyu Kim, S. Bae, Y. Yi, M. Jin Park, S. Jin Kim, N. Myoung, C.-L. Lee, B. Hee Hong, J. Hyeok Park, Origin of White Electroluminescence in Graphene Quantum Dots Embedded Host/Guest Polymer Light Emitting Diodes. *Sci. Rep.* **5**, 11032 (2015).
20. S. Ham, Y. Kim, M. J. Park, B. H. Hong, D.-J. Jang, Graphene quantum dots-decorated ZnS nanobelts with highly efficient photocatalytic performances. *RSC Adv.* **6**, 24115-24120 (2016).
21. U. Sim, J. Moon, J. An, J. H. Kang, S. E. Jerng, J. Moon, S.-P. Cho, B. H. Hong, K. T. Nam, N-doped graphene quantum sheets on silicon nanowire photocathodes for hydrogen production. *Energy Environ. Sci.* **8**, 1329-1338 (2015).
22. U. Sim, T.-Y. Yang, J. Moon, J. An, J. Hwang, J.-H. Seo, J. Lee, K. Y. Kim, J. Lee, S. Han, B. H. Hong, K. T. Nam, N-doped monolayer graphene catalyst on silicon photocathode for hydrogen production. *Energy Environ. Sci.* **6**, 3658-3664 (2013).
23. J. Park, J. Moon, C. Kim, J. H. Kang, E. Lim, J. Park, K. J. Lee, S.-H. Yu, J.-H. Seo, J. Lee, J. Heo, N. Tanaka, S.-P. Cho, J. Pyun, J. Cabana, B. H. Hong, Y.-E. Sung, Graphene quantum dots: structural integrity and oxygen functional groups for high sulfur/sulfide utilization in lithium sulfur batteries. *NPG Asia Materials* **8**, e272-e272 (2016).
24. S. Wang, I. S. Cole, Q. Li, The toxicity of graphene quantum dots. *RSC Adv.* **6**, 89867-89878 (2016).
25. L. Ou, B. Song, H. Liang, J. Liu, X. Feng, B. Deng, T. Sun, L. Shao, Toxicity of graphene-family nanoparticles: a general review of the origins and mechanisms. *Part. Fibre Toxicol.* **13**, 57 (2016).
26. D. A. Jasim, C. Ménard-Moyon, D. Bégin, A. Bianco, K. Kostarelos, Tissue distribution and urinary excretion of intravenously administered chemically functionalized graphene oxide sheets. *Chemical Science* **6**, 3952-3964 (2015).
27. J. Ma, R. Liu, X. Wang, Q. Liu, Y. Chen, R. P. Valle, Y. Y. Zuo, T. Xia, S. Liu, Crucial Role of Lateral Size for Graphene Oxide in Activating Macrophages and Stimulating Pro-inflammatory Responses in Cells and Animals. *ACS Nano* **9**, 10498-10515 (2015).
28. Y. Chong, Y. Ma, H. Shen, X. Tu, X. Zhou, J. Xu, J. Dai, S. Fan, Z. Zhang, The in vitro and in vivo toxicity of graphene quantum dots. *Biomaterials* **35**, 5041-5048 (2014).
29. O. Gamucci, A. Bertero, M. Gagliardi, G. Bardi, Biomedical Nanoparticles: Overview of Their Surface Immune-Compatibility. *Coatings* **4**, 139-159 (2014).
30. A. Sukhanova, S. Bozrova, P. Sokolov, M. Berestovoy, A. Karaulov, I. Nabiev,

Dependence of Nanoparticle Toxicity on Their Physical and Chemical Properties. *Nanoscale Research Letters* **13**, 44 (2018).

31. Y. Liu, J. Hardie, X. Zhang, V. M. Rotello, Effects of engineered nanoparticles on the innate immune system. *Semin. Immunol.* **34**, 25-32 (2017).
32. Y. Zhou, H. Sun, F. Wang, J. Ren, X. Qu, How functional groups influence the ROS generation and cytotoxicity of graphene quantum dots. *ChemComm* **53**, 10588-10591 (2017).
33. J. Dong, K. Wang, L. Sun, B. Sun, M. Yang, H. Chen, Y. Wang, J. Sun, L. Dong, Application of graphene quantum dots for simultaneous fluorescence imaging and tumor-targeted drug delivery. *Sensors Actuators B: Chem.* **256**, 616-623 (2018).
34. T. A. Tabish, C. J. Scotton, D. C. J. Ferguson, L. Lin, A. v. d. Veen, S. Lowry, M. Ali, F. Jabeen, M. Ali, P. G. Winyard, S. Zhang, Biocompatibility and toxicity of graphene quantum dots for potential application in photodynamic therapy. *Nanomedicine* **13**, 1923-1937 (2018).
35. D. Kim, J. M. Yoo, H. Hwang, J. Lee, S. H. Lee, S. P. Yun, M. J. Park, M. Lee, S. Choi, S. H. Kwon, S. Lee, S.-H. Kwon, S. Kim, Y. J. Park, M. Kinoshita, Y.-H. Lee, S. Shin, S. R. Paik, S. J. Lee, S. Lee, B. H. Hong, H. S. Ko, Graphene quantum dots prevent α-synucleinopathy in Parkinson's disease. *Nat. Nanotechnol* **13**, 812-818 (2018).
36. I. Kang, J. M. Yoo, D. Kim, J. Kim, M. K. Cho, S.-E. Lee, D. J. Kim, B.-C. Lee, J. Y. Lee, J.-J. Kim, N. Shin, S. W. Choi, Y.-H. Lee, H. S. Ko, S. Shin, B. H. Hong, K.-S. Kang, Graphene Quantum Dots Alleviate Impaired Functions in Niemann-Pick Disease Type C in Vivo. *Nano Lett.*, (2021).
37. B.-C. Lee, J. Y. Lee, J. Kim, J. M. Yoo, I. Kang, J.-J. Kim, N. Shin, D. J. Kim, S. W. Choi, D. Kim, B. H. Hong, K.-S. Kang, Graphene quantum dots as anti-inflammatory therapy for colitis. *Sci. Adv.* **6**, eaaz2630 (2020).
38. B. Zhang, P. Wei, Z. Zhou, T. Wei, Interactions of graphene with mammalian cells: Molecular mechanisms and biomedical insights. *Adv. Drug Del. Rev.* **105**, 145-162 (2016).
39. M. Orecchioni, C. Ménard-Moyon, L. G. Delogu, A. Bianco, Graphene and the immune system: Challenges and potentiality. *Adv. Drug Del. Rev.* **105**, 163-175 (2016).
40. A. E. Nel, L. Mädler, D. Velegol, T. Xia, E. M. V. Hoek, P. Somasundaran, F. Klaessig, V. Castranova, M. Thompson, Understanding biophysicochemical interactions at the nano–bio interface. *Nat. Mater.* **8**, 543-557 (2009).
41. M. A. Dobrovolskaia, S. E. McNeil, Immunological properties of engineered nanomaterials. *Nat. Nanotechnol* **2**, 469-478 (2007).
42. J. Peng, W. Gao, B. K. Gupta, Z. Liu, R. Romero-Aburto, L. Ge, L. Song, L. B. Alemany, X. Zhan, G. Gao, S. A. Vithayathil, B. A. Kaipparettu, A. A. Marti, T. Hayashi, J.-J. Zhu, P. M. Ajayan, Graphene Quantum Dots Derived from Carbon Fibers. *Nano Lett.* **12**, 844-849 (2012).
43. K. N. Kudin, B. Ozbas, H. C. Schniepp, R. K. Prud'homme, I. A. Aksay, R. Car, Raman Spectra of Graphite Oxide and Functionalized Graphene Sheets. *Nano Lett.* **8**, 36-41 (2008).
44. D. N. H. Tran, S. Kabiri, D. Losic, A green approach for the reduction of graphene oxide nanosheets using non-aromatic amino acids. *Carbon* **76**, 193-202 (2014).

45. F. Yuan, L. Ding, Y. Li, X. Li, L. Fan, S. Zhou, D. Fang, S. Yang, Multicolor fluorescent graphene quantum dots colorimetrically responsive to all-pH and a wide temperature range. *Nanoscale* **7**, 11727-11733 (2015).
46. M. C. Duch, G. S. Budinger, Y. T. Liang, S. Soberanes, D. Urich, S. E. Chiarella, L. A. Campochiaro, A. Gonzalez, N. S. Chandel, M. C. Hersam, Minimizing oxidation and stable nanoscale dispersion improves the biocompatibility of graphene in the lung. *Nano Lett.* **11**, 5201-5207 (2011).
47. K. Yang, J. Wan, S. Zhang, Y. Zhang, S.-T. Lee, Z. Liu, In vivo pharmacokinetics, long-term biodistribution, and toxicology of PEGylated graphene in mice. *ACS nano* **5**, 516-522 (2011).
48. D. C. Marcano, D. V. Kosynkin, J. M. Berlin, A. Sinitskii, Z. Sun, A. Slesarev, L. B. Alemany, W. Lu, J. M. Tour, Improved Synthesis of Graphene Oxide. *ACS Nano* **4**, 4806-4814 (2010).
49. J. Han, Y. S. Kim, M.-Y. Lim, H. Y. Kim, S. Kong, M. Kang, Y. W. Choo, J. H. Jun, S. Ryu, H.-y. Jeong, J. Park, G.-J. Jeong, J.-C. Lee, G. H. Eom, Y. Ahn, B.-S. Kim, Dual Roles of Graphene Oxide To Attenuate Inflammation and Elicit Timely Polarization of Macrophage Phenotypes for Cardiac Repair. *ACS Nano* **12**, 1959-1977 (2018).
50. V. Volarevic, V. Paunovic, Z. Markovic, B. Simovic Markovic, M. Misirkic-Marjanovic, B. Todorovic-Markovic, S. Bojic, L. Vucicevic, S. Jovanovic, N. Arsenijevic, I. Holclajtner-Antunovic, M. Milosavljevic, M. Dramicanin, T. Kravic-Stevovic, D. Ciric, M. L. Lukic, V. Trajkovic, Large Graphene Quantum Dots Alleviate Immune-Mediated Liver Damage. *ACS Nano* **8**, 12098-12109 (2014).
51. Y. Qin, Z.-W. Zhou, S.-T. Pan, Z.-X. He, X. Zhang, J.-X. Qiu, W. Duan, T. Yang, S.-F. Zhou, Graphene quantum dots induce apoptosis, autophagy, and inflammatory response via p38 mitogen-activated protein kinase and nuclear factor-κB mediated signaling pathways in activated THP-1 macrophages. *Toxicology* **327**, 62-76 (2015).
52. H. Yue, W. Wei, Z. Yue, B. Wang, N. Luo, Y. Gao, D. Ma, G. Ma, Z. Su, The role of the lateral dimension of graphene oxide in the regulation of cellular responses. *Biomaterials* **33**, 4013-4021 (2012).
53. B. Homayun, X. Lin, H.-J. Choi, Challenges and recent progress in oral drug delivery systems for biopharmaceuticals. *Pharmaceutics* **11**, 129 (2019).
54. L. Liu, W. Yao, Y. Rao, X. Lu, J. Gao, pH-Responsive carriers for oral drug delivery: challenges and opportunities of current platforms. *Drug Deliv.* **24**, 569-581 (2017).
55. Y. Yoshioka, Characterization of carbonyl chloride-terminated aromatic polyamide nanoparticles with carboxyl groups and their reaction. *Int. J. Polym. Anal. Charact.* **23**, 537-544 (2018).
56. W. W. Kaeding, Oxidation of Aromatic Acids. IV. Decarboxylation of Salicylic Acids. *The Journal of Organic Chemistry* **29**, 2556-2559 (1964).
57. D. Guarnieri, P. Sánchez-Moreno, A. E. Del Rio Castillo, F. Bonaccorso, F. Gatto, G. Bardi, C. Martín, E. Vázquez, T. Catelani, S. Sabella, Biotransformation and biological interaction of graphene and graphene oxide during simulated oral ingestion. *Small* **14**, 1800227 (2018).
58. S. Priyadarsini, S. Mohanty, S. Mukherjee, S. Basu, M. Mishra, Graphene and graphene oxide as nanomaterials for medicine and biology application. *J Nanostructure Chem* **8**, 123-137 (2018).

59. N. Luo, J. K. Weber, S. Wang, B. Luan, H. Yue, X. Xi, J. Du, Z. Yang, W. Wei, R. Zhou, PEGylated graphene oxide elicits strong immunological responses despite surface passivation. *Nat. Commun.* **8**, 1-10 (2017).
60. C. Meng, X. Zhi, C. Li, C. Li, Z. Chen, X. Qiu, C. Ding, L. Ma, H. Lu, D. Chen, Graphene oxides decorated with carnosine as an adjuvant to modulate innate immune and improve adaptive immunity in vivo. *ACS nano* **10**, 2203-2213 (2016).
61. S. K. Singh, M. K. Singh, P. P. Kulkarni, V. K. Sonkar, J. J. Grácio, D. Dash, Amine-modified graphene: thrombo-protective safer alternative to graphene oxide for biomedical applications. *ACS nano* **6**, 2731-2740 (2012).
62. Y. Chong, Y. Ma, H. Shen, X. Tu, X. Zhou, J. Xu, J. Dai, S. Fan, Z. Zhang, The in vitro and in vivo toxicity of graphene quantum dots. *Biomaterials* **35**, 5041-5048 (2014).
63. K. Yang, H. Gong, X. Shi, J. Wan, Y. Zhang, Z. Liu, In vivo biodistribution and toxicology of functionalized nano-graphene oxide in mice after oral and intraperitoneal administration. *Biomaterials* **34**, 2787-2795 (2013).
64. C. Martín, G. Jun, R. Schurhammer, G. Reina, P. Chen, A. Bianco, C. Ménard-Moyon, Enzymatic Degradation of Graphene Quantum Dots by Human Peroxidases. *Small* **15**, 1905405 (2019).
65. L. Yu, X. Tian, D. Gao, Y. Lang, X.-X. Zhang, C. Yang, M.-M. Gu, J. Shi, P.-K. Zhou, Z.-F. Shang, Oral administration of hydroxylated-graphene quantum dots induces intestinal injury accompanying the loss of intestinal stem cells and proliferative progenitor cells. *Nanotoxicology* **13**, 1409-1421 (2019).
66. M. Zheng, J. Lu, G. Lin, H. Su, J. Sun, T. Luan, Dysbiosis of gut microbiota by dietary exposure of three graphene-family materials in zebrafish (Danio rerio). *Environ. Pollut.* **254**, 112969 (2019).
67. J. Li, S. Yang, J. Yu, R. Cui, R. Liu, R. Lei, Y. Chang, H. Geng, Y. Qin, W. Gu, S. Xia, K. Chen, J. Kong, G. Chen, C. Wu, G. Xing, Lipid- and gut microbiota-modulating effects of graphene oxide nanoparticles in high-fat diet-induced hyperlipidemic mice. *RSC Adv.* **8**, 31366-31371 (2018).
68. B. C. Lee, J. J. Kim, J. Y. Lee, I. Kang, N. Shin, S. E. Lee, S. W. Choi, J. Y. Cho, H. S. Kim, K. S. Kang, Disease-specific primed human adult stem cells effectively ameliorate experimental atopic dermatitis in mice. *Theranostics* **9**, 3608-3621 (2019).

Appendix

Education

2018.3 ~ 2021.2 | Master of Science, Department of Chemistry, College of Natural Sciences, Seoul National University, Seoul, Republic of Korea.

2016.1 ~ 2016.5 | Exchange Student Program, University of North Carolina at Chapel Hill, NC

2014.3 ~ 2018.2 | Bachelor of Science, Department of Chemistry, Korea University, Seoul, Republic of Korea

Honors and Awards

2019.3 ~ 2020.7 | Global Ph.D. Fellowship granted by the National Research Foundation of Korea

2019.6 | Certificate of Commendation (outstanding teaching assistant) - Seoul National University

2019.6 | Outstanding Graduate Teaching Assistant Award - Seoul National University

Peer-Reviewed Publications

- B. –C. Lee†, J.Y. Lee†, **J. Kim**, J.M. Yoo, I. Kang, J. Kim, N. Shin, D.J. Kim, S.W. Choi, D. Kim, B.H. Hong*, K. Kang* - "Graphene quantum dots as anti-inflammatory therapy for colitis"
  B. –C. Lee et al., 2020, *Sci. Adv.* **6** : eaaz2630

- **J. Kim**†, B. Park†, D.H. Shin†, J.M. Yoo, H. Lee*, B.H. Hong* - "Photocatalytic degradation of phenol using Chemical Vapor Deposition graphene column"
  J. Kim et al., 2020, *Catalysts* **10**(11), 1251

- I. Kang†, J. M. Yoo†, D. Kim, **J. Kim**, M.K. Cho, S.E. Lee, D.J. Kim, B. –C. Lee, J. Y. Lee, J. –J. Kim, N. Shin, S.W. Choi, Y. –H. Lee, HS. Ko, S. Shin, B. H.

Hong*, and K. -S. Kang*. - “Graphene quantum dots alleviate impaired functions in Niemann-Pick disease type C in vivo.
I. Kang et al., 2021, *Nano Lett,* doi.org/10.1021/acs.nanolett.0c03741

Manuscripts under review / in preparation

- B.-C. Lee†, J.Y. Lee†, **J. Kim**†, N. Shin, J.M. Yoo, I. Kang, J.-J. Kim, S.-E. Lee, D. Kim, S.W. Choi, B.H. Hong*, K.-S. Kang* - “Oral administration of microbiome-friendly graphene quantum dots as therapy for colitis” (Submitted)

Abstract in Korean

초록

그래핀 양자점 합성 및 분석과
염증성 장질환에서의 적용

서울대학교 대학원

화학부 물리화학 전공

김 주 희

그래핀 기반 나노물질은 특성을 조절하기 쉽고 안정하기 때문에 광촉매, 디스플레이, 에너지 저장 장치 등에 적용되었다. 그 중, 산화 그래핀과 그래핀 양자점은 그 특성에 따라 높은 생체적합성과 낮은 독성을 갖는 것으로 알려져 있다. 또한, 이러한 물질들은 매우 뛰어난 항산화 효과를 띄기 때문에 주변의 활성산소 라디칼을 안정화할 수 있음으로 다양한 염증성 질환에 적용되었다. 독성은 크기, 표면 전하, 투여 농도 등에 따라 변하기 때문에 적합한 용도 맞도록 특성을 조절하는 것이 필수적이다. 일부 그래핀 기반 나노물질은 빛을 조사했을 때 매우 높은 강도의 형광을 방출하기 때문에 바이오 이미징 기법에도 적용이 가능하며, 표면적이 넓기 때문에 약물 전달을 위한 매개체로 사용되기도 한다. 최근에 그래핀 양자점은 발병성 단백질인 알파 시뉴클레인과 물리적으로 상호작용하는 것이 밝혀졌는데, 이미 형성된 알파시뉴클레인

섬유를 분해하거나, 섬유화 과정 자체를 억제함으로써 파킨슨병의 새로운 치료제로서의 가능성을 보였다. 이러한 그래핀 양자점의 질병에 치료제로서의 적용 사례를 기반으로 이 논문은 두 가지 크기의 그래핀 양자점의 합성과 분석법과 염증성 장 질환에 치료제로서 적용한 연구에 관해 설명한다.

1장은 두 가지 크기의 그래핀 양자점의 합성과 특성 분석에 대한 설명으로 시작한다. 그래핀 양자점의 생물 의학적 적용에 집중하여, 산화 그래핀과 그래핀 양자점의 항산화 및 항균 효과에 관해 설명하였다. 그 후, 그래핀 양자점이 다양한 질환 모델에 적용된 사례를 소개하며, 이번 연구의 질환 모델인 염증성 장 질환에 대한 설명도 포함하였다. 그래핀 양자점의 생체적합성과 독성은 다양한 요인에 의해 변하기 때문에, 물리 화학적 특성과 투여 경로에 따라 독성 정도가 다른 점을 강조하였다.

2장에서는 염증성 장 질환 중 하나인 궤양성 대장염에 크기가 비교적 큰 그래핀 양자점을 치료 목적으로 적용한 연구에 대한 결과이다. 본 연구는 서울대학교 수의과대학과 공동 연구를 통해 그래핀 기반 나노물질이 면역계 질환에 어떠한 영향을 미치는지에 대해 밝혔다. 그래핀 양자점을 Dextran Sodium Sulfate로 유도한 궤양성 대장염 마우스 모델에 복강 주사로 투여하였다. 그래핀 양자점은 과한 염증반응을 완화하고, 다양한 면역세포와의 상호작용을 통해 면역 항상성을 복구할 수 있었다. 그래핀 양자점을 건강한 마우스에 투여했을 때는, 뚜렷한 독성이 발견되지 않았으며, 소변을 통해 체외로 배출되는 것을 확인하였다.

3장에서는 작은 그래핀 양자점을 같은 궤양성 대장염 마우스 모델에 경구로 투여하여 효능을 확인한 연구의 결과이다. 마찬가지로, 그래핀 양자점은 다른 크기와 투여 경로에도 불구하고 독성을 확인할 수 없었다. 그래핀 양자점을 경구로 전달하면서, 위산에 노출되기 때문에 염산 용액에 그래핀 양자점을 분산시킨 후, 물질의 특성 변화를 분석하였다. 결과적으로 두 가지 크기의 그래핀 양자점을 두 가지 경로로 투여했을 때 모두 염증성 장 질환에서의 효능을 보여 새로운 치료제로서의 가능성을 보였다.

중심어: 그래핀, 그래핀 기반 나노 물질, 산화 그래핀, 그래핀 양자점, 염증성 장 질환, 궤양성 대장염

학번: 2018-26779